Article

Cell Reports

Gasdermin D Exerts Anti-inflammatory Effects by Promoting Neutrophil Death

Graphical Abstract

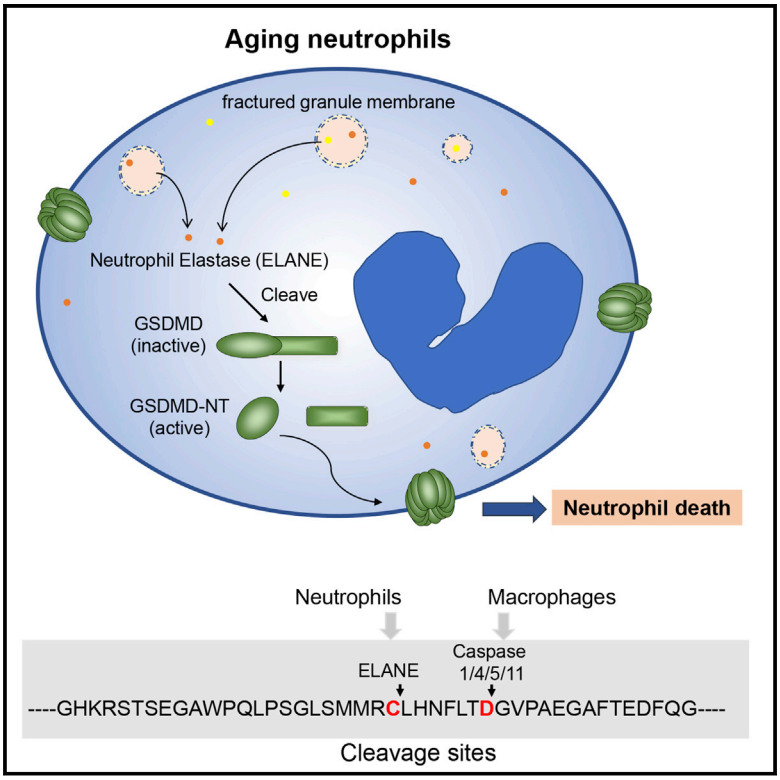

Highlights

- GSDMD-deficient mice display augmented bactericidal activity against *Escherichia coli*
- GSDMD is a key regulator of neutrophil death
- Delayed neutrophil death leads to enhanced host defense in GSDMD-deficient mice
- GSDMD cleavage in neutrophils is mediated by neutrophil elastase

Authors

Hiroto Kambara, Fei Liu, Xiaoyu Zhang, ..., Mingzhe Han, Yuanfu Xu, Hongbo R. Luo

Correspondence

hongbo.luo@childrens.harvard.edu

In Brief

Kambara et al. find that GSDMD deficiency augments host responses to extracellular *Escherichia coli*, mainly by delaying neutrophil death, establishing GSDMD as a negative regulator of innate immunity. GSDMD cleavage and activation in neutrophils is mediated by ELANE, released from cytoplasmic granules into the cytosol in aging neutrophils.

Kambara et al., 2018, Cell Reports *22*, 2924–2936
March 13, 2018
https://doi.org/10.1016/j.celrep.2018.02.067

CellPress

OPEN ACCESS
CellPress

Cell Reports
Article

Gasdermin D Exerts Anti-inflammatory Effects by Promoting Neutrophil Death

Hiroto Kambara,[1,2,7] Fei Liu,[3,7] Xiaoyu Zhang,[1,2,3,7] Peng Liu,[3] Besnik Bajrami,[4] Yan Teng,[1,2] Li Zhao,[1,2] Shiyi Zhou,[1,2] Hongbo Yu,[5] Weidong Zhou,[6] Leslie E. Silberstein,[1,2] Tao Cheng,[3] Mingzhe Han,[3] Yuanfu Xu,[3] and Hongbo R. Luo[1,2,8,*]

[1]Department of Pathology, Harvard Medical School, Dana-Farber/Harvard Cancer Center, Boston, MA 02215, USA
[2]Department of Laboratory Medicine, Children's Hospital Boston, Enders Research Building, Room 814, Boston, MA 02115, USA
[3]The State Key Laboratory of Experimental Hematology, Institute of Hematology and Blood Diseases Hospital, Chinese Academy of Medical Sciences and Peking Union Medical College, 288 Nanjing Road, Tianjin 300020, China
[4]Center for Development of Therapeutics, Broad Institute, 415 Main Street, Cambridge, MA 02142, USA
[5]VA Boston Healthcare System, Department of Pathology and Laboratory Medicine, Harvard Medical School, 1400 VFW Parkway, West Roxbury, MA 02132, USA
[6]Center for Applied Proteomics and Molecular Medicine, George Mason University, Manassas, VA 20110, USA
[7]These authors contributed equally
[8]Lead Contact
*Correspondence: hongbo.luo@childrens.harvard.edu
https://doi.org/10.1016/j.celrep.2018.02.067

SUMMARY

Gasdermin D (GSDMD) is considered a proinflammatory factor that mediates pyroptosis in macrophages to protect hosts from intracellular bacteria. Here, we reveal that GSDMD deficiency paradoxically augmented host responses to extracellular *Escherichia coli*, mainly by delaying neutrophil death, which established GSDMD as a negative regulator of innate immunity. In contrast to its activation in macrophages, in which activated inflammatory caspases cleave GSDMD to produce an N-terminal fragment (GSDMD-cNT) to trigger pyroptosis, GSDMD cleavage and activation in neutrophils was caspase independent. It was mediated by a neutrophil-specific serine protease, neutrophil elastase (ELANE), released from cytoplasmic granules into the cytosol in aging neutrophils. ELANE-mediated GSDMD cleavage was upstream of the caspase cleavage site and produced a fully active ELANE-derived NT fragment (GSDMD-eNT) that induced lytic cell death as efficiently as GSDMD-cNT. Thus, GSDMD is pleiotropic, exerting both pro- and anti-inflammatory effects that make it a potential target for antibacterial and anti-inflammatory therapies.

INTRODUCTION

Neutrophils are terminally differentiated cells and have a short lifespan in circulation and tissue (Lahoz-Beneytez et al., 2016; Lord et al., 2001). Neutrophil death plays a critical role in regulating neutrophil numbers in infection and inflammation. Aging neutrophils undergo programmed death and are then recognized, engulfed, and safely cleared by professional phagocytes such as macrophages (Savill et al., 1989). Neutrophil death shares many features of classical apoptosis and involves caspase activation. However, it is not entirely caspase dependent. Inhibition of caspases, which are critical mediators of apoptosis, delays but does not completely abolish cell death, suggesting that other mechanisms of neutrophil death exist (Loison et al., 2014; Luo and Loison, 2008).

Gasdermin D (GSDMD) was recently identified as the factor responsible for the inflammatory form of lytic pyroptotic cell death, a critical antibacterial innate immune defense mechanism (He et al., 2015; Kayagaki et al., 2015; Shi et al., 2015a). Activated inflammatory caspases (caspase-1/4/5/11) cleave GSDMD in macrophages to produce an N-terminal fragment (GSDMD-cNT) that triggers pyroptosis by binding to phosphatidylinositol phosphates and phosphatidylserine in the cell membrane inner leaflet to induce membrane pore formation and interleukin-1β (IL-1β) secretion (Aglietti et al., 2016; Chen et al., 2016; Ding et al., 2016; He et al., 2015; Liu et al., 2016; Sborgi et al., 2016). GSDMD-cNT also binds to cardiolipin in the inner and outer leaflets of bacterial membranes, suggesting that it may directly kill bacteria by perforating bacterial membranes (Ding et al., 2016; Liu et al., 2016). Based on these studies, GSDMD is generally considered proinflammatory and an important host response to bacterial infection. Although GSDMD-deficient mice are protected from lethal endotoxemia (Kayagaki et al., 2015; Shi et al., 2015a), their bactericidal capability against extracellular pathogens has not been examined directly.

Here, we reveal that GSDMD deficiency unexpectedly and paradoxically augments host defenses against extracellular *Escherichia coli* by delaying neutrophil death. Its cleavage and activation in neutrophils is caspase independent, instead mediated by a neutrophil-specific serine protease, neutrophil elastase (ELANE), and released from neutrophil granules into the cytosol during neutrophil death. GSDMD controls neutrophil death and negatively regulates neutrophil-mediated innate immunity. Thus, GSDMD can exert context-dependent proinflammatory and anti-inflammatory effects and is a unique target for antibacterial and anti-inflammatory therapies.

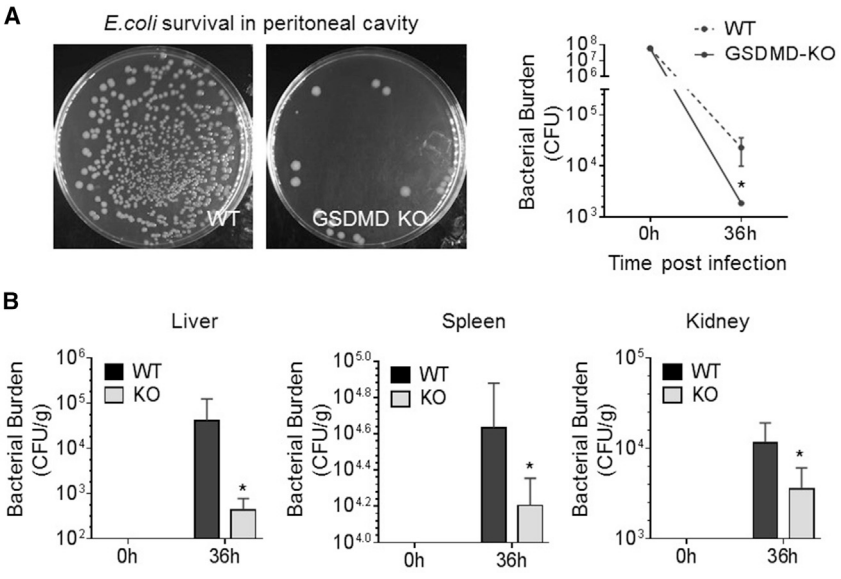

Figure 1. GSDMD-Deficient Mice Display Augmented Bactericidal Activity

(A) *E. coli* clearance in inflamed peritoneal cavities. Live bacteria were quantified as total colony-forming units (CFU) in peritoneal lavage fluid (PLF).

(B) Total CFUs in the indicated organs and peripheral blood 36 hr after *E. coli* challenge.

RESULTS

GSDMD-Deficient Mice Display Augmented Bactericidal Activity against *E. coli*

Pyroptosis often occurs when macrophages are infected with intracellular pathogens and is thought to be critical for the clearance of these pathogens (Jorgensen and Miao, 2015; Jorgensen et al., 2016). Whether GSDMD contributes to the general bactericidal activity in host defense and the potential mechanism leading to its activation during this process remains elusive. We therefore explored bacterial killing in wild-type (WT) and GSDMD-deficient mice (Figures S1A–S1E) in a murine acute peritoneal infection (peritonitis) model (Li et al., 2009). As previously reported, *Gsdmd*$^{-/-}$ mice were viable, fertile, and of normal size; peripheral blood differential counts were normal; and blood smears showed no hematopoietic abnormalities (Figures S1F–S1H). We then assessed the survival of WT and knockout (KO) mice in a lipopolysaccharide (LPS)-induced sepsis model. Consistent with the published results, our GSDMD-deficient mice also showed significantly improved survival compared to the WT mice (Figure S1I).

In this model, the host defenses suppress bacterial proliferation and gradually clear the intraperitoneally injected Gram-negative *E. coli*. 36 hr after injection of 5 × 10^7 live *E. coli*, the number of viable bacteria in peritoneal cavities consistently reduced to 2 × 10^4 in WT mice, reflecting a functioning immune system. Significantly fewer bacteria (1.8 × 10^3) were detected in inflamed GSDMD-deficient mice, suggesting that host responses to bacteria are enhanced in these mice (Figure 1A). Bacteria disseminate widely in infected hosts during severe infection, but, consistent with enhanced host immune responses in GSDMD-deficient mice, bacterial loads also were significantly reduced in the spleens, livers, and kidneys of GSDMD-deficient mice compared to WT mice (Figure 1B). WT mice also displayed marked splenomegaly, another sign typical of bacterial infection (Figures S1J and S1K). Infection-associated splenomegaly was alleviated significantly in the GSDMD-deficient mice. Collectively, GSDMD disruption appears to augment host bactericidal activity to *E. coli* infection, indicating that GSDMD may be a negative regulator of innate immunity.

The Augmented Host Antibacterial Response in GSDMD-Deficient Mice Is the Result of Enhanced Neutrophil Accumulation

Enhanced bacterial killing may be the result of enhanced phagocytosis of bacteria by neutrophils. We first assessed neutrophil phagocytosis capability using mouse bone marrow neutrophils. GSDMD deficiency did not alter phagocytosis efficiency as measured by the percentage of neutrophils that engulfed at least one *E. coli* bioparticle (Figure 2A). The phagocytosis index of GSDMD-deficient neutrophils also was comparable to that of WT neutrophils: nearly 100 bacteria were engulfed by 100 neutrophils (Figure 2A). We next examined whether GSDMD disruption intrinsically alters the bactericidal capability of neutrophils *in vitro* using purified WT and GSDMD-deficient neutrophils, but GSDMD-deficient neutrophils were equally as efficient as WT neutrophils at clearing live *E. coli* (Figure 2B). The intracellular bactericidal activity of neutrophils was further assessed by treating samples with a plasma membrane-impermeable antibiotic that kills extracellular bacteria but not internalized intracellular bacteria. The same number of viable engulfed bacteria was detected in both GSDMD-deficient and WT neutrophils, suggesting that GSDMD does not directly regulate the killing of intracellular bacteria (Figure 2B). Thus, the increased bactericidal activity observed in GSDMD-deficient mice does not appear to occur because the intrinsic bacterial killing capability of each neutrophil is enhanced. Similar results were observed when phagocytosis and bacterial killing capability were examined in peripheral blood neutrophils (Figures 2C and 2D).

Elevated bacterial killing also may be caused by enhanced neutrophil accumulation in the inflamed peritoneal cavity. Few peritoneal neutrophils were present in unchallenged mice; however, after *E. coli* injection, the number of peritoneal neutrophils increased to the same extent in both WT and GSDMD-deficient mice to nearly 9 × 10^6 after 24 hr (Figure 2E). GSDMD deficiency does not, therefore, affect initial neutrophil recruitment, but GSDMD-deficient mice did show drastic increases in *E. coli*-induced neutrophil accumulation (15 × 10^6 versus 7 × 10^6 neutrophils in *Gsdmd*$^{-/-}$ versus WT mice, respectively) 48 hr after *E. coli* injection (Figure 2E). Therefore, the augmented host antibacterial response in GSDMD-deficient mice is likely to

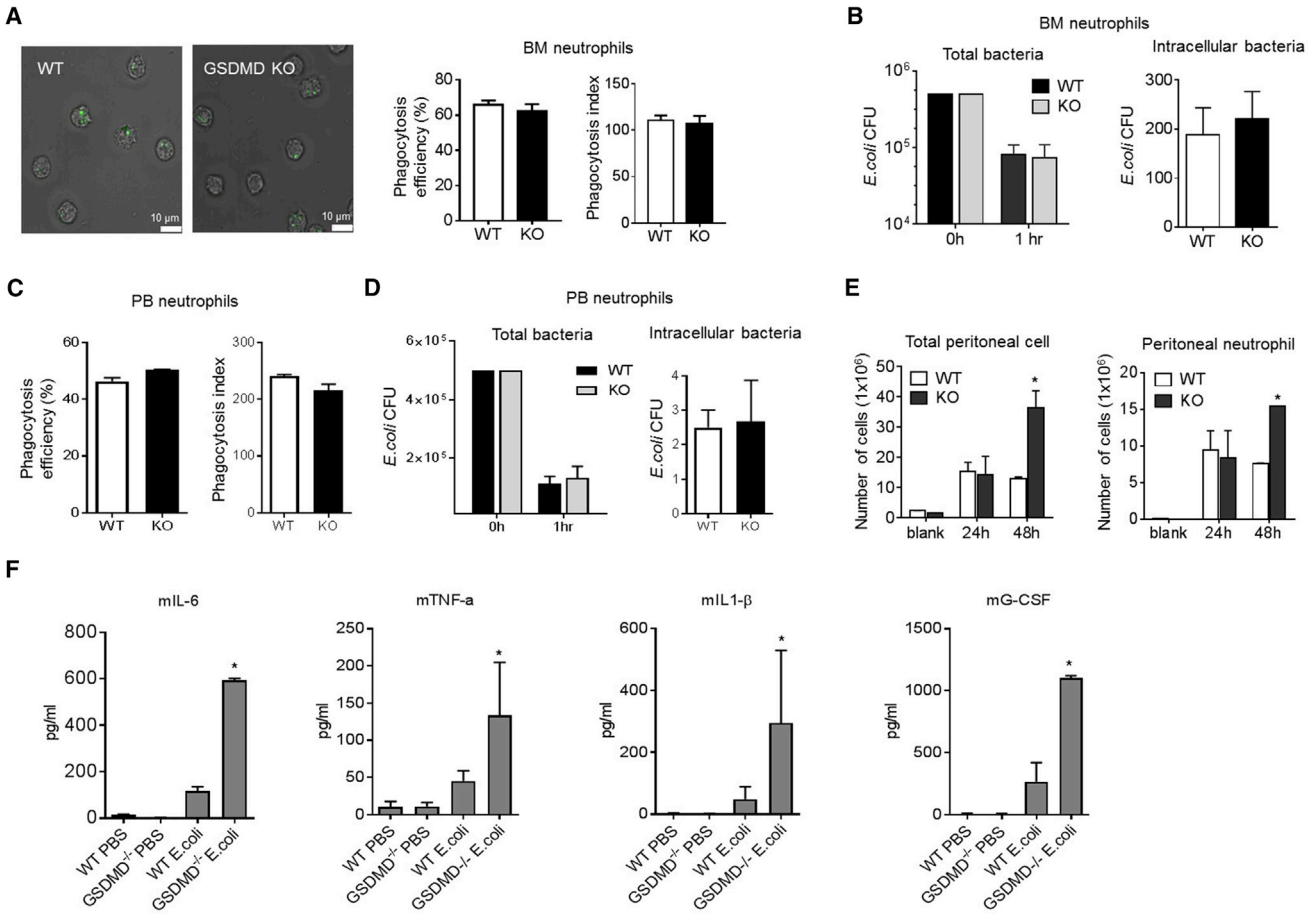

Figure 2. The Augmented Host Antibacterial Response in GSDMD-Deficient Mice Is the Result of Enhanced Neutrophil Accumulation

(A) *In vitro* phagocytosis assay. More than 200 neutrophils were counted in each group.

(B) *In vitro* killing of *E. coli* by bone marrow neutrophils. *In vitro* bacterial killing capabilities were reflected by the decrease in CFUs. Intracellular bactericidal activity of neutrophils was assessed by treating samples with kanamycin to kill extracellular bacteria.

(C) Phagocytosis of *E. coli* bioparticles by peripheral blood neutrophils. Results are the means (±SDs) of three independent experiments.

(D) *In vitro* killing of *E. coli* by peripheral blood neutrophils. Results are the means (±SDs) of three independent experiments.

(E) Total peritoneal cell and peritoneal neutrophil numbers in *E. coli*-challenged mice. Data shown at each time point are means ± SDs of four mice.

(F) Chemokine and cytokine levels in peritoneal cavity.

Results are the means (±SDs) of three independent experiments. *p < 0.05 versus WT.

be the result of enhanced neutrophil accumulation in the inflamed peritoneal cavity rather than an enhanced intrinsic capacity of neutrophils to kill bacteria. Thus, under this condition, GSDMD acted as an anti-inflammatory factor. Consistently, the levels of proinflammatory cytokines in the peritoneal cavity were elevated significantly in *Gsdmd*$^{-/-}$ mice, suggesting that the production of these cytokines was not mediated mainly by macrophage pyroptosis (Figure 2F).

Delayed Neutrophil Death Led to Elevated Neutrophil Accumulation and Enhanced Host Defenses in *Gsdmd*$^{-/-}$ Mice

Elevated neutrophil accumulation at sites of infection can occur simply as a result of enhanced neutrophil recruitment from the circulation to the inflamed peritoneal cavity, but the unaltered peritoneal neutrophil counts during the early stage of bacterial infection make this unlikely. In addition, we measured the peripheral neutrophil count before and after infection (Figure S2A). No difference was detected between the WT and GSDMD-deficient mice. In the bacterial peritonitis model, neutrophil recruitment can be regulated indirectly by the number of live bacteria remaining in the peritoneal cavity, which was reduced in GSDMD-deficient mice. Thus, to directly assess neutrophil recruitment during inflammation, we induced sterile peritonitis with thioglycolate (TG), which more rapidly elicited neutrophil recruitment than the bacterial model to reach a peak 7 hr after injection (Li et al., 2011). Again, similar numbers of peritoneal neutrophils were detected in WT and GSDMD-deficient mice at this early phase of inflammation, confirming that GSDMD deficiency does not alter neutrophil recruitment (Figures 3A and 3B). Furthermore, we measured the number of both resident and inflammatory macrophages in the peritoneal cavity. No difference was

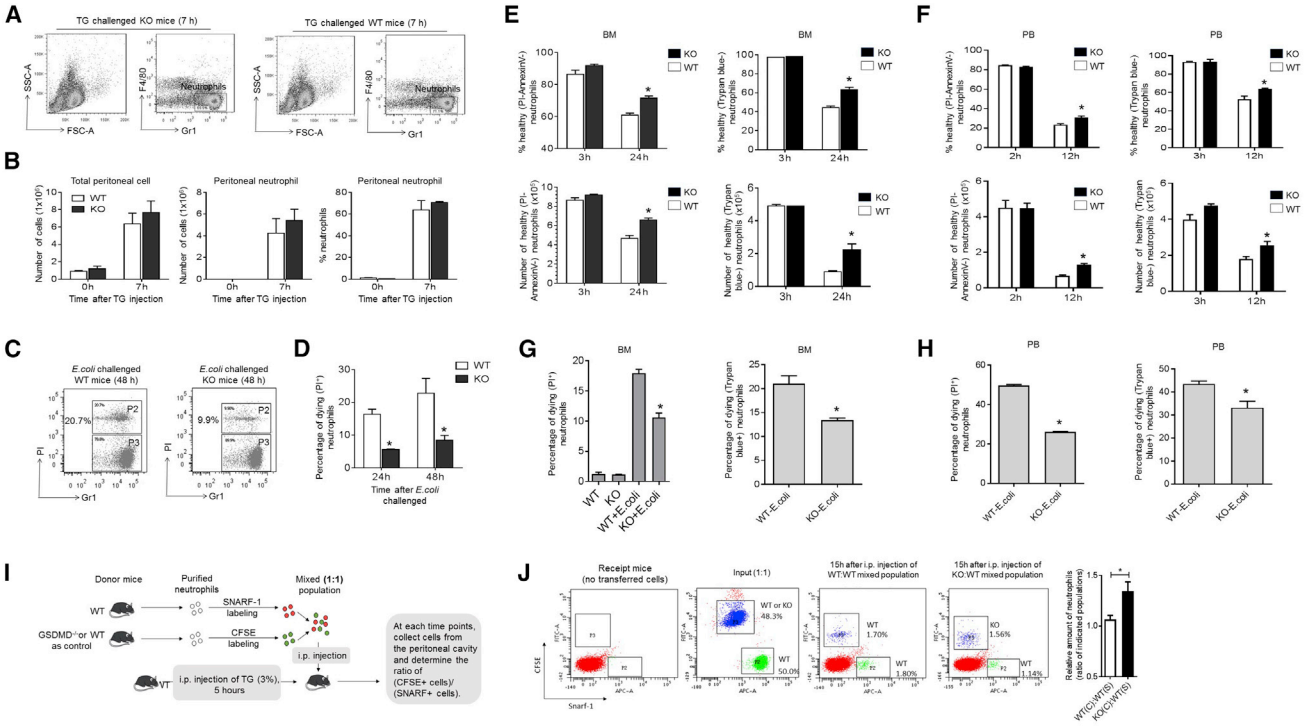

Figure 3. Delayed Neutrophil Death Elevates Neutrophil Accumulation and Enhances the Host Defense Response in GSDMD-Deficient Mice

(A) Neutrophil recruitment during sterile inflammation. At the indicated times, TG-challenged mice were killed and peritoneal lavage fluid collected for FACS. Shown are representative FACS plots depicting recruited peritoneal neutrophils.

(B) Total neutrophil content in the lavage fluid was calculated based on FACS analysis. Data shown at each time point are means ± SDs of three mice.

(C) Neutrophil death during *E. coli*-induced peritonitis. Peritoneal cells were collected 48 hr after *E. coli* injection and then analyzed by FACS. Shown are representative FACS plots depicting dying peritoneal neutrophils (P2). See also Figures S2D and S2E.

(D) The percentage of dying neutrophils in the lavage fluid was calculated based on FACS analysis. Data shown at each time point are means ± SDs of three mice.

(E) Death of *in vitro* cultured WT and GSDMD-deficient bone marrow neutrophils. Shown are the percentage and absolute number of healthy neutrophils in the culture at time points indicated. Data shown are means ± SDs of three mice. See also Figures S3A–S3D.

(F) Death of *in vitro* cultured WT and GSDMD-deficient peripheral blood neutrophils. All of the values represent means ± SDs of three separate experiments.

(G) Death of *in vitro* cultured WT and GSDMD-deficient bone marrow neutrophils in the presence of *E. coli.* Bone marrow neutrophils were cultured with *E. coli* (1:5 ratio) for 2 hr. Data shown are means ± SDs of three mice.

(H) Death of *in vitro* cultured WT and GSDMD-deficient peripheral blood neutrophils in the presence of *E. coli.* Data shown are means ± SDs of three mice.

(I) *In vivo* death of adoptively transferred neutrophils.

(J) The ratios of adoptively transferred WT and GSDMD-deficient neutrophils. The input control was normalized to 1, and the results shown are the ratios at 15 hr after the adoptive transfer.

All of the values represent means ± SDs. *$p < 0.05$ versus WT.

detected between the WT and GSDMD-deficient mice (Figure S2B). In addition, using an *in vitro* assay we examined the clearance of dead neutrophils by macrophages, a process known as efferocytosis (Poon et al., 2014). GSDMD disruption in macrophages did not affect efferocytosis efficiency (Figure S2C). We therefore speculated that the elevated neutrophil accumulation during late-stage infection was caused by a prolonged lifespan of recruited neutrophils.

We next explored whether neutrophil death is delayed in the peritoneal cavities of GSDMD-deficient mice. We measured the percentage of dying neutrophils in peritoneal lavage fluid (PLF) by fluorescence-activated cell sorting (FACS) analysis (Figure 3C, S2D, and S3E). Although apoptotic neutrophils can be engulfed and cleared by macrophages, there were still >20% dying neutrophils (propidium iodide-positive [PI^+] cells) in the inflamed peritoneal cavities of WT mice 48 hr after *E. coli* injection compared to only 8% dying neutrophils in GSDMD-deficient mice. Notably, the decrease of dying neutrophil number in GSDMD-deficient mice was already detectable at 24 hr after *E. coli* injection before the total neutrophil number had started to decline (Figure 3D). Delayed neutrophil death may, therefore, be responsible for augmented neutrophil accumulation in GSDMD-deficient mice.

A reduction in dying peritoneal neutrophils could be the result of an altered peritoneal inflammatory environment, exaggerated clearance by peritoneal macrophages, or both. We next used a well-established *in vitro* system to determine whether delayed *in vivo* neutrophil death was indeed caused by alterations in intrinsic death/survival pathways in GSDMD-deficient neutrophils (Xu et al., 2010) (Figure S3A). Neutrophils die even in the absence of any stimuli. Thus, this type of death also is called neutrophil spontaneous or constitutive death. We first explored whether neutrophil constitutive death is delayed in a GSDMD-deficient

neutrophil population. Freshly isolated GSDMD-deficient bone marrow or peripheral blood neutrophils were morphologically normal (Figure S3B). However, consistent with the *in vivo* results, *in vitro*-cultured GSDMD-deficient bone marrow neutrophils showed delayed spontaneous death compared to WT neutrophils, with 40% more healthy neutrophils in the GSDMD-deficient neutrophil population compared to WT (Figures 3E and S3C). Similar results were observed in peripheral blood neutrophils (Figure 3F). In the presence of *E. coli*, neutrophils die much faster.

We also examined the role of GSDMD in *E. coli*-induced neutrophil death, a process mediated mainly by phagocytosis. Again, we observed significantly delayed death in the GSDMD-deficient neutrophil population (Figures 3G, 3H, and S3D). Finally, we used an adoptive transfer assay to investigate whether GSDMD is involved intrinsically in neutrophil death *in vivo* (Figures 3I and 3J). In this assay, fluorescent-labeled WT and GSDMD-deficient neutrophils were injected directly into the peritoneal cavity of the same recipient mice so that we were able to assess the survival and death of WT and GSDMD-deficient neutrophils in the same environment. Consistent with the *ex vivo* data, significantly more GSDMD-deficient neutrophils were detected in the inflamed peritoneal cavity compared to WT neutrophils 15 hr after the adoptive transfer (Figures 3I and 3J). The results of this experiment directly confirm that GSDMD disruption in neutrophils can intrinsically lead to delayed neutrophil death *in vivo* at the site of inflammation.

We also investigated whether GSDMD plays a role in neutrophil recruitment. Fluorescent-labeled WT and GSDMD-deficient neutrophils were injected into an TG-challenged WT receipt intravenously. Peritoneal neutrophil number was assessed at earlier time points when neutrophil death had not yet occurred. The ratio of WT to GSDMD-deficient neutrophils in the inflamed peritoneal cavity remained unaltered compared to the input (1:1), indicating that disruption of GSDMD in neutrophils did not affect neutrophil recruitment during infection and inflammation (Figures S3E and S3F).

GSDMD Cleavage and Activation in Neutrophils Is Mediated by ELANE in a Caspase-Independent Manner

Our results suggest that GSDMD may play a role in regulating neutrophil death. To further explore this hypothesis, we first investigated GSDMD expression in neutrophils. Examination of two publicly available transcriptomes of hematopoietic cells revealed that GSDMD is highly expressed in neutrophils at levels comparable to those in macrophages (Figures S4A and S4B). Consistent with this, GSDMD protein was present in both highly purified neutrophils and neutrophil-like differentiated HL60 cells (Figures 4A and 4B).

During macrophage pyroptosis, caspases cleave full-length GSDMD. To explore GSDMD cleavage activity in neutrophils, we incubated recombinant FLAG-tagged full-length GSDMD (FLAG-FL-GSDMD) with neutrophil lysate, thereby allowing us to track the cleaved NT GSDMD fragments. GSDMD could be processed by both human (Figure 4C) and mouse (Figure 4D) neutrophil lysates to generate an NT fragment of similar size to GSDMD-cNT. To investigate whether cleavage was caspase dependent, we included Z-Tyr-Val-Ala-Asp(OMe)-fluoromethylketone (z-YVAD-fmk), a caspase inhibitor, in the cleavage reaction. z-YVAD-fmk efficiently blocked caspase-elicited GSDMD cleavage as expected (Loison et al., 2014), but it failed to suppress human (Figure 4E) or mouse (Figure 4F) neutrophil lysate-elicited GSDMD cleavage, suggesting that GSDMD cleavage by neutrophil lysate was caspase independent. Noticeably, human neutrophil lysate degraded all of the GSDMD protein species. Compared to the input, there was virtually no human GSDMD-NT (hGSDMD-NT) left after 30 min. Instead, the mouse lysate generated a stable mouse GSDMD-NT (mGSDMD-NT) fragment. The rapid degradation of hGSDMD-NT could be caused by other proteases in human neutrophil lysate. We wondered whether GSDMD was cleaved by neutrophil serine proteases to generate an active GSDMD-NT fragment. To test this, neutrophil lysates were treated with diisopropylfluorophosphate (DFP), a potent and irreversible serine protease inhibitor. DFP treatment significantly reduced both human and mouse neutrophil lysate-induced GSDMD cleavage (Figures 4E and 4F). Thus, GSDMD cleavage and activation in neutrophils is caspase independent and is likely to be mediated by a serine protease.

To determine which serine protease may be responsible for GSDMD cleavage and activation, we incubated FLAG-hGSDMD with caspase-1 and each of the three major neutrophil serine proteases: proteinase 3 (PR3), ELANE, and cathepsin G. As previously reported, caspase-1 cleaved FL-GSDMD to generate GSDMD-cNT. We were intrigued that one of the neutrophil serine proteases, ELANE, also cleaved GSDMD to generate a GSDMD-NT fragment (GSDMD-eNT) that was slightly smaller than GSDMD-cNT. In contrast, PR3 and cathepsin G failed to produce a significant number, if any, of GSDMD-NT fragments (Figure 4G). Several cleaved bands were detected by an antibody recognizing GSDMD, perhaps representing non-specific and non-functional cleavage in the middle of GSDMD (Figure S4C). The degree of GSDMD cleavage was positively correlated with ELANE enzymatic activity in the reaction (Figure S4D), and the cleavage was efficiently inhibited by ELANE-specific inhibitors sivelestat (Figure S4E), BAY-678 (Figure S4F), and GW311616A (Figure S4G) and by the pan-serine protease inhibitor DFP (Figure S4H). More important, GSDMD cleavage by whole human neutrophil lysate also was reduced significantly by ELANE-specific inhibitors in a dose-dependent manner (Figure 4H), and the GSDMD-NT fragment produced by neutrophil lysate was the same size as the one cleaved by ELANE (Figures S4I and S4J). Therefore, GSDMD cleavage activity in human neutrophil lysate appears to be attributable mainly to ELANE.

We next sought to investigate whether ELANE also mediates mGSDMD cleavage. Active recombinant mouse ELANE is not commercially available, so we incubated ELANE precursor with active cathepsin C/dipeptidylpeptidase I (DPPI), which removes dipeptide from the ELANE precursor to generate active mature ELANE (Adkison et al., 2002). In parallel to ELANE activation, mGSDMD was processed into two major NT fragments, one of which was a similar size to that of GSDMD-cNT (Figure 4I). ELANE-specific protease inhibitors inhibited generation of this fragment in a dose-dependent manner (Figure S4K), as did ELANE-deficient neutrophil lysate (Figure 4J). Thus, both mouse and human ELANE can effectively and efficiently cleave GSDMD to produce GSDMD-eNT in neutrophils. As a control, caspase-1/11 double KO (DKO) neutrophil lysate cleaved mGSDMD as

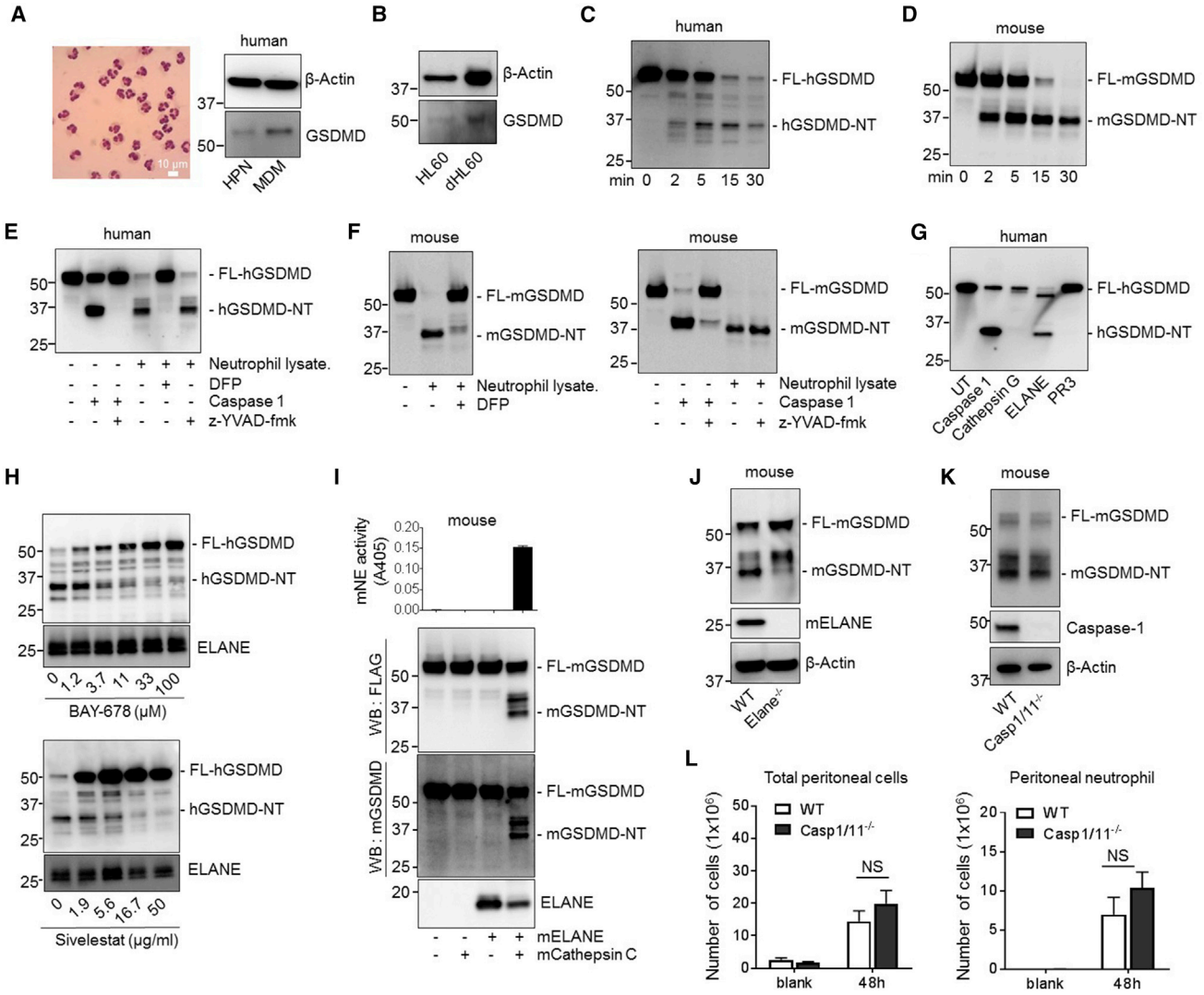

Figure 4. The Cleavage and Activation of GSDMD in Neutrophils Is Mediated by ELANE in a Caspase-Independent Manner

(A) GSDMD is highly expressed in neutrophils. GSDMD in human neutrophils and monocyte-derived macrophages (MDMs) was detected by western blotting with anti-GSDMD antibody. The purity of highly purified neutrophils (HPNs) was confirmed by Wright-Giemsa staining of cytospin samples.

(B) GSDMD expression in undifferentiated and differentiated HL60 cells.

(C) Cleavage of human GSDMD (hGSDMD) by human neutrophil lysate. FLAG-hGSDMD was overexpressed in HEK293T cells. Cell lysates containing recombinant FLAG-hGSDMD were incubated with human neutrophil lysate for the times indicated. The positions of the full-length (FL-GSDMD) and ELANE-cleaved N-terminal hGSDMD (hGSDMD-NT) are indicated.

(D) Cleavage of mouse GSDMD (mGSDMD) by mouse neutrophil lysate. FLAG-mGSDMD was overexpressed in HEK293T cells and was incubated with mouse neutrophil lysate for the times indicated.

(E) hGSDMD cleavage by human neutrophil lysate was mediated by serine proteases. The cleavage of FLAG-hGSDMD by caspase-1 or human neutrophil lysate was conducted as described in Figure 4C in the presence of indicated inhibitors.

(F) The cleavage of mGSDMD by mouse neutrophil lysate in the presence of caspase or serine protease inhibitor.

(G) The cleavage of hGSDMD by serine proteases. FLAG-hGSDMD was overexpressed in HEK293T cells. Cell lysates containing recombinant FLAG-hGSDMD were incubated with human recombinant caspase 1 (100 units), PR3 (2 μg), ELANE (2 μg), or cathepsin G (2 μg) at 37°C for 30 min in a 6-well plate. The positions of the FL- and ELANE-cleaved hGSDMD are indicated.

(H) The cleavage of hGSDMD by human neutrophil lysate in the presence of the indicated number of ELANE-specific inhibitors.

(I) The cleavage of mGSDMD by mouse ELANE. FLAG-mGSDMD was overexpressed in HEK293T cells and incubated with the indicated proteases. ELANE enzymatic activity was determined using an ELANE-specific substrate following the manufacturer's protocol.

(J) The cleavage of mGSDMD by ELANE-deficient neutrophil lysate. Disruption of ELANE was confirmed by western blotting with ELANE antibody.

(K) The cleavage of mGSDMD by caspase-1/11-deficient neutrophil lysate.

(L) Total peritoneal cell and peritoneal neutrophil numbers in *E. coli*-challenged WT and caspase-1/11-deficient mice. Total neutrophil content in the lavage fluid was calculated by FACS analysis.

Data shown at each time point are means ± SDs of four mice. NS, not significant; $p > 0.05$ versus WT.

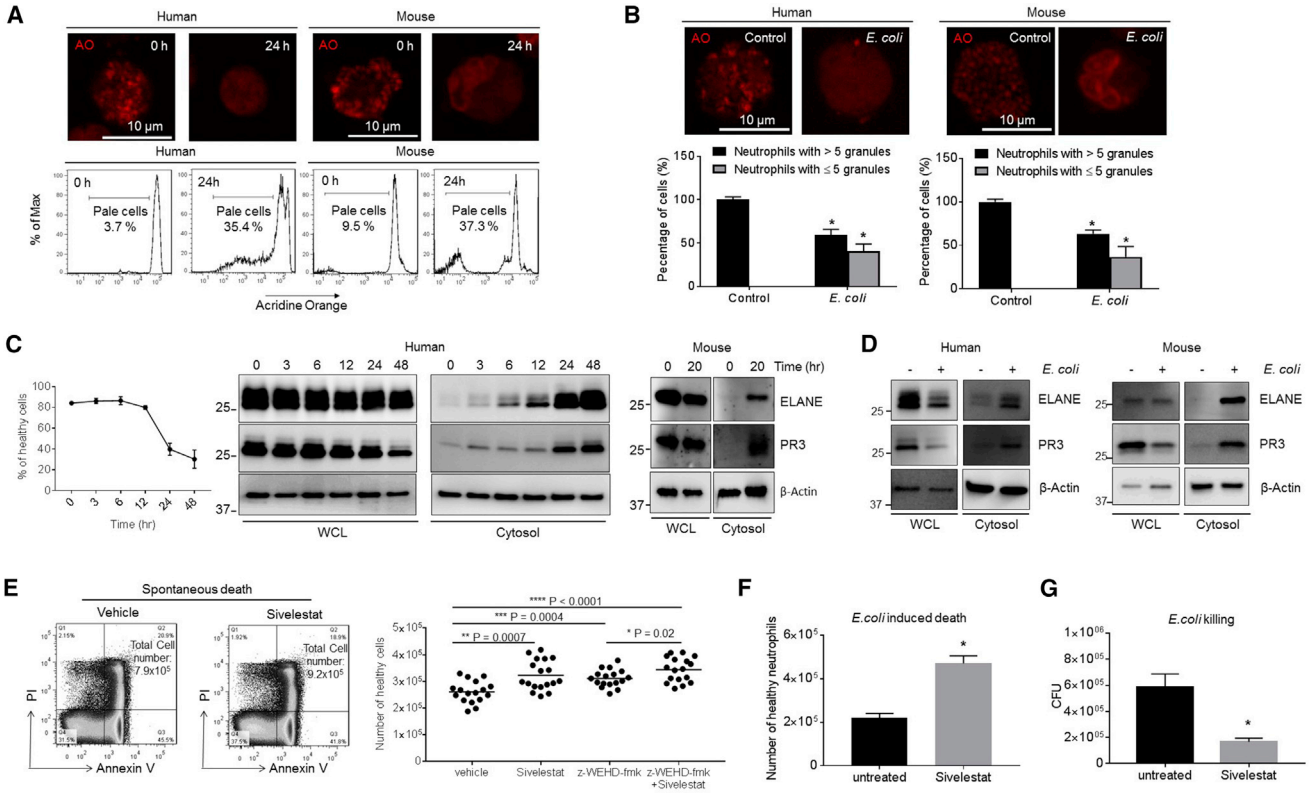

Figure 5. Lysosomal Membrane Permeabilization Induces ELANE Release into the Cytosol and the Subsequent GSDMD Cleavage

(A) Neutrophil lysosomal membrane permeabilization (LMP) was assessed using the acridine orange (AO) uptake assay after 24 hr of culture. Shown are representative images and FACS plots of three independent experiments.

(B) *E. coli*-induced LMP. Mouse or human neutrophils were cultured with opsonized *E. coli* (1:5 ratio) for 30 min. Cells containing ≥5 granules and cells containing <5 granules are calculated. Shown are representative images of three independent experiments.

(C) PR3 and ELANE protein expression in whole-cell lysates (WCL) and the cytosolic fraction of fresh and aging neutrophils. Shown are representative blots of three independent experiments.

(D) PR3 and ELANE protein expression in neutrophils treated with *E. coli*. Human and mouse neutrophils were cultured with opsonized *E. coli* (1:5 ratio) for 60 min. Shown are representative blots of three independent experiments.

(E) Spontaneous neutrophil death in the presence of ELANE, caspase-1/4/5-specific inhibitors, or all of these. Human primary neutrophils were isolated and cultured in the presence of ELANE-specific inhibitor sivelestat (1 μg/mL), caspase-1/4/5-specific inhibitor z-WEHD-fmk (10 μM), or all of these for 26 hr. All of the values represent means ± SDs.

(F) *E. coli*-induced neutrophil death in the presence of ELANE inhibitor. Human neutrophils were cultured with opsonized *E. coli* (1:5 ratio) in the presence of sivelestat (1 μg/mL) for 60 min. All of the values represent means ± SDs of three experiments.

(G) *In vitro* killing of *E. coli* by aged human neutrophils. Human primary neutrophils were isolated and cultured in the presence of ELANE-specific inhibitor sivelestat (1 μg/mL) for 26 hr. The cultured aged neutrophils were then incubated with *E. coli* for 1 hr. *In vitro* bacterial killing capabilities were reflected by the decrease in CFU after indicated incubation periods.

All of the values represent means ± SDs of three experiments. *p < 0.05 versus control.

efficiently as the WT neutrophil lysate, further indicating that GSDMD cleavage in neutrophils is caspase-1/11-independent (Figure 4K). Caspase-1/11 DKO mice consistently did not exhibit significantly elevated neutrophil accumulation in the peritonitis model, again confirming that the elevated neutrophil accumulation observed in the GSDMD-deficient KO is caspase-1/11 independent (Figure 4L).

Lysosomal Membrane Permeabilization Induces ELANE Release into the Cytosol, Leading to GSDMD Cleavage

GSDMD must co-localize with ELANE in neutrophils for cleavage, so we next examined this activity. In healthy neutrophils, the cytoplasmic granules mediate antimicrobial activity and contain all three serine proteinases, with the granule contents released during neutrophil death via lysosomal membrane permeabilization (LMP) (Figure 5A) (Loison et al., 2014). LMP was triggered in both spontaneous and *E. coli*-induced neutrophil death (Figures 5A and 5B). Cytosolic ELANE was consistently low in fresh healthy neutrophils and increased significantly during neutrophil death (Figures 5C and 5D), supporting a model in which LMP-induced ELANE release into the cytosol leads to GSDMD cleavage to facilitate neutrophil death. Indeed, we previously showed that the inhibition of LMP drastically delays constitutive neutrophil death (Loison et al., 2014). Consistent with our hypothesis, treatment with ELANE-specific inhibitor delayed significantly the death program in human neutrophils

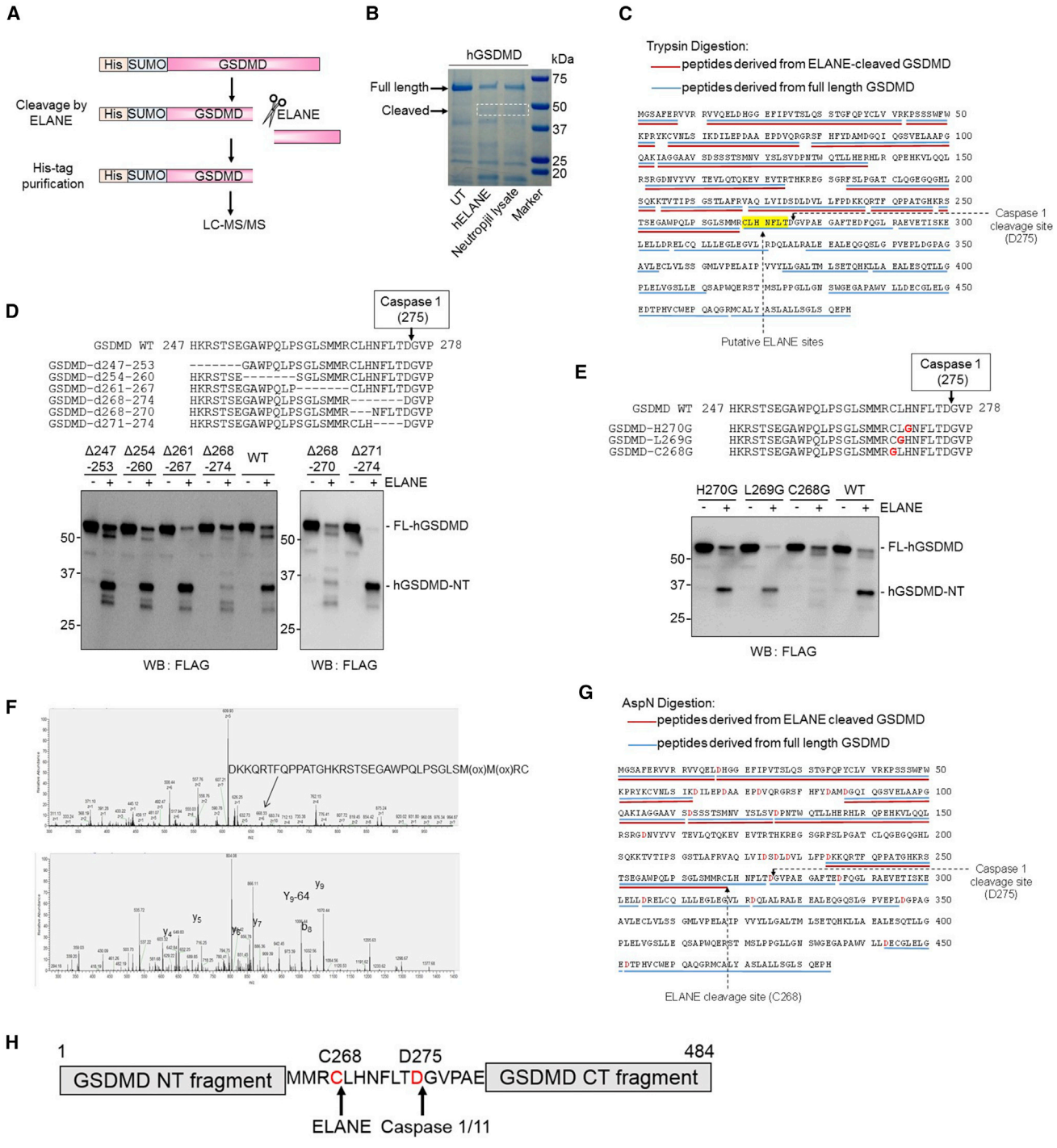

Figure 6. ELANE Cleaves GSDMD Upstream of the Caspase Cleavage Site

(A) Schematic ofGSDMD cleavage by ELANE and the strategy for identifying the cleavage site by mass spectrometry (MS).

(B) Recombinant human His-SUMO-GSDMD was incubated with ELANE or human neutrophil lysates at 37°C for 30 min and subjected to SDS-PAGE followed by colloidal blue staining. The FL and ELANE-cleaved GSDMD-NT fragment were trypsin digested and analyzed by MS.

(C) Trypsin-digested peptides derived from the FL (blue lines) and ELANE-cleaved (red lines) GSDMD are underlined. The putative ELANE cleavage sites are highlighted.

(D) The cleavage of hGSDMD deletion mutants by ELANE. The FLAG-tagged hGSDMD deletion mutants were overexpressed in HEK293T cells. ELANE-mediated hGSDMD cleavage was carried out and analyzed as described in Figure 4C.

(E) The cleavage of hGSDMD point mutants by ELANE. Results are representative of four independent experiments.

(legend continued on next page)

(Figure 5E). In addition, treatment with ELANE inhibitor could further promote the survival of neutrophils treated with the caspase-1/4/5-specific inhibitor, indicating that the effect of ELANE is independent of caspase-mediated GSDMD cleavage. Thus, ELANE appears to be a key regulatory protease that cleaves GSDMD to produce GSDMD-eNT during neutrophil death. Similar to what was observed in spontaneous neutrophil death, treatment with ELANE inhibitor also could promote the survival of cultured human neutrophils in the presence of *E. coli* infection (Figure 5F). It is noteworthy that ELANE inhibitor-induced suppression of neutrophil death was not as prominent as the one elicited by GSDMD disruption, indicating that ELANE may not be the only protease that cleaves and activates GSDMD in neutrophils. We next examined the bacterial killing capability of the untreated and ELANE inhibitor-treated neutrophil cultures (Figure 5G). ELANE inhibitor-induced delayed death of cultured human neutrophils led to augmented bacterial killing, consistent with the increased healthy neutrophil number in these cultures. We next assessed the neutrophil chemotaxis capability using a EZ-TAXIScan (ECI Frontier Inc) device (Hattori et al., 2010). It is interesting that the chemotaxis and phagocytosis capabilities of the surviving cells were unaltered (Figures S5A and S5B). This is consistent with the well-accepted mechanism by which GSDMD mediates cell death. The transiently generated GSDMD-NT triggers neutrophil death immediately upon its generation, leading to the attenuated overall bacterial killing capability of neutrophil culture. However, the surviving cells likely do not contain high levels of GSDMD-NT and thus function normally.

ELANE Cleaves GSDMD Upstream of the Caspase Cleavage Site to Generate a Smaller but Still Biologically Active GSDMD-eNT Fragment

GSDMD-eNT is slightly smaller than GSDMD-cNT on western blots. To determine the exact ELANE cutting site on GSDMD, we produced both human and mouse recombinant His-SUMO-GSDMD in *E. coli*, using the NT GSDMD-His-SUMO tag fusion to specifically purify GSDMD-eNT fragments after cleavage for subsequent mass spectrometry (MS) (Figure 6A). hGSDMD was incubated with ELANE or human neutrophil lysate, and intact and cleaved GSDMD bands were excised and subjected to liquid chromatography-MS (Figure 6B). Analysis of trypsin-digested fragments derived from FL-hGSDMD and hGSDMD-eNT localized the cleavage site to a seven-amino acid sequence between 268 and 274 (Figure 6C). We then generated a series of hGSDMD deletion mutants between amino acids 247 and 282. GSDMD-Δ268–274 and -Δ268–270 failed to be cleaved efficiently by ELANE, suggesting that the cleavage site localizes between C268 and H270 (Figure 6D). Because glycine is found rarely at ELANE cleavage sites and is thought to be an amino acid that cannot be cleaved by ELANE (Camper et al., 2016), we made glycine point mutants at 268, 269, and 270. GSDMD-C268G but not other GSDMD mutants generated significantly less GSDMD-eNT in response to treatment with ELANE (Figure 6E), pinpointing the ELANE cleavage site on hGSDMD to C268 and further confirming by MS analysis AspN-digested hGSDMD fragments. A peptide ending at C268 was identified in the GSDMD-eNT sample but not in the sample containing FL-hGSDMD (Figures 6F and 6G). The identified ELANE cleavage site, C268, was seven amino acids upstream of the caspase cleavage site D275 (Figure 6H). Using a similar approach, we revealed that mGSDMD was cleaved at V251 (Figures S6A–S6F). Notably, the GSDMD ELANE cleavage site was not well conserved between humans and mice (Figure S6G), suggesting that ELANE may recognize a tertiary structure rather than a particular amino acid sequence in GSDMD. These results are consistent with the known preference of ELANE for small hydrophobic amino acids such as Val, Cys, and Ala at the P1 position of protein substrates (Korkmaz et al., 2008).

The ELANE and caspase cleavage sites in GSDMD are, therefore, different. We next examined whether ELANE-mediated GSDMD cleavage also activates it by expressing human GSDMD-eNT (hGSDMD 1–268) and GSDMD-cNT (hGSDMD 1–275) in 293T cells (Figure 7A). GSDMD-NT-mediated plasma membrane pore formation depends on the oligomerization of GSDMD-NT molecules. Both hGSDMD-eNT and hGSDMD-cNT efficiently formed oligomers (Figure 7B) and localized to the plasma membrane (Figure 7C). Both hGSDMD-eNT and hGSDMD-cNT but not the FL or hGSDMD1 to 225, a truncated inactive form of hGSDMD, consistently induced lytic death of 293T cells (Figure 7D). The dying cells displayed typical lytic morphology of cell swelling and rupture and leakage of the plasma membrane, leading to intracellular DNA staining by membrane-impermeable PI (Movies S1, S2, S3, and S4). In addition, death-associated release of lactate dehydrogenase (LDH) also was comparable between hGSDMD-eNT- and hGSDMD-cNT-expressing cells (Figure 7E). Similar cytotoxicity also was observed when mGSDMD-eNTs (mGSDMD1–251) were expressed in 293T cells (Figures S7A and S7B). Collectively, these results show that ELANE-cleaved GSDMD is biologically active and induces lytic cell death, which are consistent with previous findings that the minimum length of active GSDMD-NT is ~243 amino acids (Shi et al., 2015a).

DISCUSSION

GSDM family proteins are inactive in their steady state because of autoinhibition by the C-terminus domain (He et al., 2015; Shi et al., 2015a; Shi et al., 2015b). Their activation relies on cleavage of the FL protein to generate the NT active fragment. GSDM cleavage may be context dependent and mediated by distinct mechanisms in different tissues and cells. ELANE-meditated GSDMD cleavage is likely to be a specific GSDMD activation mechanism in neutrophils because other cell types, including monocyte-derived

(F) MS analysis of the ELANE cleavage site in hGSDMD was conducted using AspN-digested samples. Top, mass spectrum of oxidized AspN-peptide generated through the cleavage. Bottom, MS/MS spectrum of the corresponding peptide showing the fragment ions detected and used for protein identification.
(G) MS analysis identifies C268 as the ELANE cleavage site in hGSDMD. AspN-digested peptides derived from the FL (blue lines) and ELANE-cleaved (red lines) GSDMD are underlined.
(H) ELANE- and caspase-1-cleaved hGSDMD at different sites.

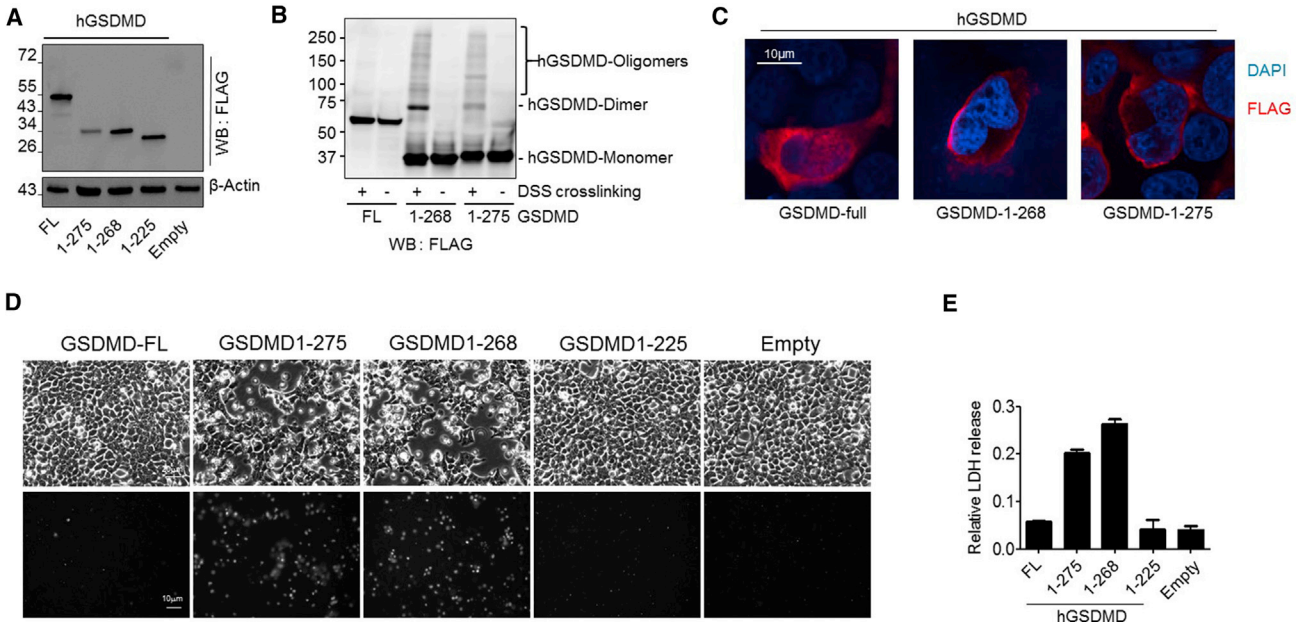

Figure 7. ELANE Cleaves GSDMD to Generate a Smaller but still Biologically Active GSDMD-eNT Fragment

(A) Expression of FLAG-tagged FL, ELANE-cleaved (hGSDMD-eNT or 1–268), and caspase-cleaved (hGSDMD-cNT or 1–275) human GSDMD in HEK293T cells. The cells were lysed 24 hr post-transfection.

(B) GSDMD protein oligomerization. The cells expressing the indicated hGSDMD protein were lysed with lysis buffer with or without disuccinimidyl suberate crosslinking reagent (1 mg/mL) and incubated at room temperature for 30 min. The reaction was quenched by 0.1 M Tris, pH 7.4.

(C) Subcellular localization of recombinant hGSDMD in 293T cells. Shown are representative images of three independent experiments.

(D) Cell morphology of transfected cells was observed by bright field microscopy 24 hr post-transfection (see also Movies S1, S2, S3, and S4). PI staining was conducted to assess cell death. Shown are representative images of three independent experiments.

(E) Cytotoxicity was measured using a lactate dehydrogenase (LDH) cytotoxicity assay. All of the values represent means ± SDs of three independent experiments.

macrophages (MDMs), do not express ELANE (Figures S7C and S7D). Alternatively, ELANE may not be the only protease that cleaves and activates GSDMD in neutrophils. An NT fragment slightly larger than GSDMD-eNT was still generated in the absence of ELANE and also may participate in lytic cell death (Figure 4J). Inflammasome-mediated caspase-1 activation has been implicated in neutrophil-mediated cytokine release and neutrophilic inflammation (Bakele et al., 2014; Chen et al., 2014; Karmakar et al., 2016), and thus may elicit GSDMD cleavage and activation in neutrophils independent of ELANE. Nevertheless, caspase-1/11 DKO neutrophil lysate cleaved mGSDMD as efficiently as the WT neutrophil lysate to generate mGSDMD-NT (Figure 4K). In addition, caspase-1/11 DKO mice did not exhibit elevated neutrophil accumulation in the peritonitis model, confirming that the elevated neutrophil accumulation observed in the GSDMD-deficient KO is caspase independent.

In macrophages, cleavage of GSDMD induces membrane pore formation and proinflammatory cytokine (e.g., IL-1β) secretion (Aglietti et al., 2016; Chen et al., 2016; Ding et al., 2016; He et al., 2015; Liu et al., 2016; Sborgi et al., 2016). GSDMD-cNT also binds to cardiolipin in the inner and outer leaflets of bacterial membranes, suggesting that it may directly kill bacteria by perforating bacterial membranes (Ding et al., 2016; Liu et al., 2016). On the basis of these studies, GSDMD is generally considered proinflammatory and an important host response to bacterial infection (Kayagaki et al., 2015; Shi et al., 2015a). Here, we reveal that GSDMD deficiency unexpectedly and paradoxically augments host defense against extracellular *E. coli* by delaying neutrophil death. GSDMD controls neutrophil death and negatively regulates neutrophil-mediated innate immunity. Because the dead neutrophils are rapidly engulfed and cleared by macrophages, this process generally reduces neutrophil number and is mainly anti-inflammatory. The levels of proinflammatory cytokines in the peritoneal cavity were elevated significantly in GSDMD-deficient mice, suggesting that the production of these cytokines was not mediated mainly by GSDMD-mediated macrophage pyroptosis. This further confirmed that in *E. coli*-induced peritonitis, GSDMD acted as an anti-inflammatory factor. Thus, GSDMD can exert context-dependent proinflammatory and anti-inflammatory effects, making it a unique target for antibacterial and anti-inflammatory therapies (Figure S7E). Although both our *in vitro* and *in vivo* data demonstrated directly that GSDMD in neutrophils can intrinsically regulate neutrophil death during infection and inflammation, we cannot completely exclude the contribution of other cell types in the regulation of neutrophil accumulation in GSDMD-deficient mice. It also is noteworthy that the effect of GSDMD disruption on neutrophil death was not as drastic as its effect on *in vivo* bacteria killing. It is likely that a modest difference in neutrophil death can upregulate inflammation, leading to more neutrophil recruitment and a log difference in bacterial clearance.

Our results support a model in which ELANE cleaves and activates GSDMD to perforate the plasma membrane and induce lytic cell death in neutrophils. It is noteworthy that depletion of GSDMD did not completely block lytic neutrophil death, suggesting that other parallel pathways exist to facilitate neutrophil death. In fact, the canonical caspase-3-mediated mechanism is well documented to regulate neutrophil death. Alternatively, other GSDM family proteins may be expressed in neutrophils and cleaved by neutrophil proteases to promote neutrophil death in the absence of GSDMD. Apoptosis has long been considered the primary mechanism of cell death for aging neutrophils, but inhibition of caspases, which are critical mediators of apoptosis, delay but do not completely abolish cell death, suggesting that other mechanisms of neutrophil death exist (Loison et al., 2014; Luo and Loison, 2008). Our most recent study showed that neutrophil death consists of not only apoptosis but also a heterogeneous collection of different types of cell death (Kasorn et al., 2009; Teng et al., 2017). Here, we show that GSDMD-mediated lytic cell death also contributes to neutrophil death.

Serine proteases, including ELANE, are stored mainly in azurophilic granules at concentrations exceeding 5 mM (Borregaard and Cowland, 1997). They are key components of the innate immune system and mediate pathogen clearance via multiple mechanisms, including direct suppression of pathogen proliferation and survival, production of antimicrobial peptides, deactivation of virulence factors, and generation of neutrophil extracellular traps (NETs) (Stapels et al., 2015; Tkalcevic et al., 2000). ELANE-mediated degradation of bacterial outer membrane protein A (OmpA) can kill bacteria directly (Belaaouaj et al., 2000). ELANE-deficient mice displayed impaired host defenses against Gram-negative bacterial sepsis (Belaaouaj et al., 1998). It is interesting that mice lacking both PR3 and ELANE have been linked to accumulation of anti-inflammatory progranulin (PGRN) and exaggerated inflammation, suggesting a cooperative interaction between serine proteases (Kessenbrock et al., 2008). Here, we discovered an alternative mechanism by which ELANE regulates innate immunity by promoting neutrophil death.

The present study further demonstrates the significance of LMP in promoting neutrophil death (Figure S7F). We previously showed that another serine protease, PR3, is released from granules into the cytosol via LMP in aging neutrophils to cleave and activate caspase-3 to cause neutrophil death (Loison et al., 2014). Inhibition of LMP significantly curtails PR3 release from neutrophil granules and consequently delays neutrophil death. Here, we show that ELANE and ELANE-mediated GSDMD cleavage are other key mechanisms that mediate LMP-elicited neutrophil death. Thus, LMP should be a legitimate target for regulating neutrophil death in infection and inflammation. The mechanism leading to LMP is still ill-defined. Reactive oxygen species (ROS) accumulate in aging neutrophils and mediate neutrophil death (Xu et al., 2013; Xu et al., 2010). ROS-induced lipid peroxidation may directly cause rupture of granule membranes and LMP. Electron microscopy examination reveals obvious granule membrane rupture in aging neutrophils (Loison et al., 2014). A recent study showed that ELANE release during NETosis also is triggered by ROS (Metzler et al., 2014). In resting neutrophils, ELANE is localized on the azurophilic granule membrane and associated with a multiprotein complex known as azurosome. Upon stimulation, oxidative burst generates ROS that in turn triggers dissociation of ELANE from azurosome into the cytosol and the subsequent translocation to the nucleus. It would be intriguing to investigate whether this azurosome-mediated mechanism also plays a role in neutrophil death and whether the azurosome-mediated pathway and LMP can regulate each other.

EXPERIMENTAL PROCEDURES

Mice

Eight- to 12-week-old male mice were used in all of the experiments. Corresponding littermates were used as WT controls in all of the experiments performed with KO mice. The Boston Children's Hospital Animal Care and Use Committee approved and monitored all of the procedures involving mice.

Neutrophil Apoptosis in the Inflamed Peritoneal Cavity

Peritonitis was induced by intraperitoneally injection with 5×10^7 *E. coli* (strain K12 BW25113) in PBS. At indicated times after injection, the mice were euthanized with CO_2. Peritoneal exudate cells were then harvested by three successive washes with 10 mL Hank's balanced salt solution (HBSS) containing 0.2% BSA and 20 mM EDTA. The cells were stained with annexin V (fluorescein isothiocyanate [FITC] labeled, Invitrogen) and PI, and cell death was then analyzed by FACS using a FACSCanto II flow cytometer (Becton Dickinson, San Jose, CA).

Statistics

Analysis of statistical significance for the indicated datasets was performed with the two-tailed Student's t test using GraphPad Prism 5 (GraphPad Software, La Jolla, CA). p values < 0.05 were considered significant.

SUPPLEMENTAL INFORMATION

Supplemental Information includes Supplemental Experimental Procedures, seven figures, and four movies and can be found with this article online at https://doi.org/10.1016/j.celrep.2018.02.067.

ACKNOWLEDGMENTS

The authors thank John Manis, Feng Shao, and Li Chai for helpful discussions, and Harry Leung for technical assistance with confocal microscopy. Y.X. is supported by grants from the National Basic Research Program of China (2015CB964903), the Chinese Academy of Medical Sciences (CAMS) Innovation Fund for Medical Sciences (2016-12M-1-003 and 2017-I2M-1-015), and the Chinese National Natural Science Foundation (31471116). F.L. is supported by a grant from the Chinese National Natural Science Foundation (31700783), the Peking Union Medical College (PUMC) Youth Fund, and the Fundamental Research Funds for the Central Universities (2017310023). H.L. is supported by NIH grants (R01AI103142, R01HL092020, and P01HL095489) and a grant from the Flight Attendant Medical Research Institute (FAMRI) (CIA 123008). pCSII-EF-RfA and pCSII-CMV-MCS-IRES2-Bsd vectors were kindly supplied by Dr. Hiroyuki Miyoshi (RIKEN BioResource Center). The pCAG-MCS2-FOS vector was kindly supplied by Dr. Eiji Morita (Hirosaki University).

AUTHOR CONTRIBUTIONS

Conceptualization, H.R.L. and H.K.; Methodology, F.L., X.Z., P.L., and H.K.; Investigation, F.L., X.Z., B.B., Y.T., L.Z., S.Z., H.Y., W.Z. and H.K.; Writing: Original Draft, H.K.; Writing: Review and Editing, H.K., F.L., X.Z., Y.X., L.E.S., and H.R.L.; Funding Acquisition, T.C., F.L., Y.X., L.E.S., and H.R.L.; Resources, T.C., M.H., Y.X., and L.S.; Supervision, T.C., M.H., Y.X., L.S., and H.R.L.

DECLARATION OF INTERESTS

The authors declare no competing interests.

Received: April 18, 2017
Revised: January 9, 2018
Accepted: February 15, 2018
Published: March 13, 2018

REFERENCES

Adkison, A.M., Raptis, S.Z., Kelley, D.G., and Pham, C.T. (2002). Dipeptidyl peptidase I activates neutrophil-derived serine proteases and regulates the development of acute experimental arthritis. J. Clin. Invest. *109*, 363–371.

Aglietti, R.A., Estevez, A., Gupta, A., Ramirez, M.G., Liu, P.S., Kayagaki, N., Ciferri, C., Dixit, V.M., and Dueber, E.C. (2016). GsdmD p30 elicited by caspase-11 during pyroptosis forms pores in membranes. Proc. Natl. Acad. Sci. USA *113*, 7858–7863.

Bakele, M., Joos, M., Burdi, S., Allgaier, N., Pöschel, S., Fehrenbacher, B., Schaller, M., Marcos, V., Kümmerle-Deschner, J., Rieber, N., et al. (2014). Localization and functionality of the inflammasome in neutrophils. J. Biol. Chem. *289*, 5320–5329.

Belaaouaj, A., McCarthy, R., Baumann, M., Gao, Z., Ley, T.J., Abraham, S.N., and Shapiro, S.D. (1998). Mice lacking neutrophil elastase reveal impaired host defense against gram negative bacterial sepsis. Nat. Med. *4*, 615–618.

Belaaouaj, A., Kim, K.S., and Shapiro, S.D. (2000). Degradation of outer membrane protein A in Escherichia coli killing by neutrophil elastase. Science *289*, 1185–1188.

Borregaard, N., and Cowland, J.B. (1997). Granules of the human neutrophilic polymorphonuclear leukocyte. Blood *89*, 3503–3521.

Camper, N., Glasgow, A.M., Osbourn, M., Quinn, D.J., Small, D.M., McLean, D.T., Lundy, F.T., Elborn, J.S., McNally, P., Ingram, R.J., et al. (2016). A secretory leukocyte protease inhibitor variant with improved activity against lung infection. Mucosal Immunol. *9*, 669–676.

Chen, K.W., Groß, C.J., Sotomayor, F.V., Stacey, K.J., Tschopp, J., Sweet, M.J., and Schroder, K. (2014). The neutrophil NLRC4 inflammasome selectively promotes IL-1β maturation without pyroptosis during acute Salmonella challenge. Cell Rep. *8*, 570–582.

Chen, X., He, W.T., Hu, L., Li, J., Fang, Y., Wang, X., Xu, X., Wang, Z., Huang, K., and Han, J. (2016). Pyroptosis is driven by non-selective gasdermin-D pore and its morphology is different from MLKL channel-mediated necroptosis. Cell Res. *26*, 1007–1020.

Ding, J., Wang, K., Liu, W., She, Y., Sun, Q., Shi, J., Sun, H., Wang, D.C., and Shao, F. (2016). Pore-forming activity and structural autoinhibition of the gasdermin family. Nature *535*, 111–116.

Hattori, H., Subramanian, K.K., Sakai, J., Jia, Y., Li, Y., Porter, T.F., Loison, F., Sarraj, B., Kasorn, A., Jo, H., et al. (2010). Small-molecule screen identifies reactive oxygen species as key regulators of neutrophil chemotaxis. Proc. Natl. Acad. Sci. USA *107*, 3546–3551.

He, W.T., Wan, H., Hu, L., Chen, P., Wang, X., Huang, Z., Yang, Z.H., Zhong, C.Q., and Han, J. (2015). Gasdermin D is an executor of pyroptosis and required for interleukin-1β secretion. Cell Res. *25*, 1285–1298.

Jorgensen, I., and Miao, E.A. (2015). Pyroptotic cell death defends against intracellular pathogens. Immunol. Rev. *265*, 130–142.

Jorgensen, I., Zhang, Y., Krantz, B.A., and Miao, E.A. (2016). Pyroptosis triggers pore-induced intracellular traps (PITs) that capture bacteria and lead to their clearance by efferocytosis. J. Exp. Med. *213*, 2113–2128.

Karmakar, M., Katsnelson, M.A., Dubyak, G.R., and Pearlman, E. (2016). Neutrophil P2X7 receptors mediate NLRP3 inflammasome-dependent IL-1β secretion in response to ATP. Nat. Commun. *7*, 10555.

Kasorn, A., Alcaide, P., Jia, Y., Subramanian, K.K., Sarraj, B., Li, Y., Loison, F., Hattori, H., Silberstein, L.E., Luscinskas, W.F., and Luo, H.R. (2009). Focal adhesion kinase regulates pathogen-killing capability and life span of neutrophils via mediating both adhesion-dependent and -independent cellular signals. J. Immunol. *183*, 1032–1043.

Kayagaki, N., Stowe, I.B., Lee, B.L., O'Rourke, K., Anderson, K., Warming, S., Cuellar, T., Haley, B., Roose-Girma, M., Phung, Q.T., et al. (2015). Caspase-11 cleaves gasdermin D for non-canonical inflammasome signalling. Nature *526*, 666–671.

Kessenbrock, K., Fröhlich, L., Sixt, M., Lämmermann, T., Pfister, H., Bateman, A., Belaaouaj, A., Ring, J., Ollert, M., Fässler, R., and Jenne, D.E. (2008). Proteinase 3 and neutrophil elastase enhance inflammation in mice by inactivating antiinflammatory progranulin. J. Clin. Invest. *118*, 2438–2447.

Korkmaz, B., Moreau, T., and Gauthier, F. (2008). Neutrophil elastase, proteinase 3 and cathepsin G: physicochemical properties, activity and physiopathological functions. Biochimie *90*, 227–242.

Lahoz-Beneytez, J., Elemans, M., Zhang, Y., Ahmed, R., Salam, A., Block, M., Niederalt, C., Asquith, B., and Macallan, D. (2016). Human neutrophil kinetics: modeling of stable isotope labeling data supports short blood neutrophil half-lives. Blood *127*, 3431–3438.

Li, Y., Jia, Y., Pichavant, M., Loison, F., Sarraj, B., Kasorn, A., You, J., Robson, B.E., Umetsu, D.T., Mizgerd, J.P., et al. (2009). Targeted deletion of tumor suppressor PTEN augments neutrophil function and enhances host defense in neutropenia-associated pneumonia. Blood *113*, 4930–4941.

Li, Y., Prasad, A., Jia, Y., Roy, S.G., Loison, F., Mondal, S., Kocjan, P., Silberstein, L.E., Ding, S., and Luo, H.R. (2011). Pretreatment with phosphatase and tensin homolog deleted on chromosome 10 (PTEN) inhibitor SF1670 augments the efficacy of granulocyte transfusion in a clinically relevant mouse model. Blood *117*, 6702–6713.

Liu, X., Zhang, Z., Ruan, J., Pan, Y., Magupalli, V.G., Wu, H., and Lieberman, J. (2016). Inflammasome-activated gasdermin D causes pyroptosis by forming membrane pores. Nature *535*, 153–158.

Loison, F., Zhu, H., Karatepe, K., Kasorn, A., Liu, P., Ye, K., Zhou, J., Cao, S., Gong, H., Jenne, D.E., et al. (2014). Proteinase 3-dependent caspase-3 cleavage modulates neutrophil death and inflammation. J. Clin. Invest. *124*, 4445–4458.

Lord, B.I., Woolford, L.B., and Molineux, G. (2001). Kinetics of neutrophil production in normal and neutropenic animals during the response to filgrastim (r-metHu G-CSF) or filgrastim SD/01 (PEG-r-metHu G-CSF). Clin. Cancer Res *7*, 2085–2090.

Luo, H.R., and Loison, F. (2008). Constitutive neutrophil apoptosis: mechanisms and regulation. Am. J. Hematol. *83*, 288–295.

Metzler, K.D., Goosmann, C., Lubojemska, A., Zychlinsky, A., and Papayannopoulos, V. (2014). A myeloperoxidase-containing complex regulates neutrophil elastase release and actin dynamics during NETosis. Cell Rep. *8*, 883–896.

Poon, I.K., Lucas, C.D., Rossi, A.G., and Ravichandran, K.S. (2014). Apoptotic cell clearance: basic biology and therapeutic potential. Nat. Rev. Immunol. *14*, 166–180.

Savill, J.S., Wyllie, A.H., Henson, J.E., Walport, M.J., Henson, P.M., and Haslett, C. (1989). Macrophage phagocytosis of aging neutrophils in inflammation. Programmed cell death in the neutrophil leads to its recognition by macrophages. J. Clin. Invest. *83*, 865–875.

Sborgi, L., Rühl, S., Mulvihill, E., Pipercevic, J., Heilig, R., Stahlberg, H., Farady, C.J., Müller, D.J., Broz, P., and Hiller, S. (2016). GSDMD membrane pore formation constitutes the mechanism of pyroptotic cell death. EMBO J. *35*, 1766–1778.

Shi, J., Zhao, Y., Wang, K., Shi, X., Wang, Y., Huang, H., Zhuang, Y., Cai, T., Wang, F., and Shao, F. (2015a). Cleavage of GSDMD by inflammatory caspases determines pyroptotic cell death. Nature *526*, 660–665.

Shi, P., Tang, A., Xian, L., Hou, S., Zou, D., Lv, Y., Huang, Z., Wang, Q., Song, A., Lin, Z., and Gao, X. (2015b). Loss of conserved Gsdma3 self-regulation causes autophagy and cell death. Biochem. J. *468*, 325–336.

Stapels, D.A., Geisbrecht, B.V., and Rooijakkers, S.H. (2015). Neutrophil serine proteases in antibacterial defense. Curr. Opin. Microbiol. *23*, 42–48.

Teng, Y., Luo, H.R., and Kambara, H. (2017). Heterogeneity of neutrophil spontaneous death. Am. J. Hematol. *92*, E156–E159.

Tkalcevic, J., Novelli, M., Phylactides, M., Iredale, J.P., Segal, A.W., and Roes, J. (2000). Impaired immunity and enhanced resistance to endotoxin in the absence of neutrophil elastase and cathepsin G. Immunity *12*, 201–210.

Xu, Y., Loison, F., and Luo, H.R. (2010). Neutrophil spontaneous death is mediated by down-regulation of autocrine signaling through GPCR, PI3Kgamma, ROS, and actin. Proc. Natl. Acad. Sci. USA *107*, 2950–2955.

Xu, Y., Li, H., Bajrami, B., Kwak, H., Cao, S., Liu, P., Zhou, J., Zhou, Y., Zhu, H., Ye, K., and Luo, H.R. (2013). Cigarette smoke (CS) and nicotine delay neutrophil spontaneous death via suppressing production of diphosphoinositol pentakisphosphate. Proc. Natl. Acad. Sci. USA *110*, 7726–7731.

Cell Reports, Volume *22*

Supplemental Information

Gasdermin D Exerts Anti-inflammatory Effects by Promoting Neutrophil Death

Hiroto Kambara, Fei Liu, Xiaoyu Zhang, Peng Liu, Besnik Bajrami, Yan Teng, Li Zhao, Shiyi Zhou, Hongbo Yu, Weidong Zhou, Leslie E. Silberstein, Tao Cheng, Mingzhe Han, Yuanfu Xu, and Hongbo R. Luo

SUPPLEMENTAL EXPERIMENTAL PROCEDURES

Mice

The GSDMD knockout (KO, *Gsdmd*$^{-/-}$) mouse was created by the Model Animal Research Center at Nanjing University (Nanjing, China) on a pure C57BL/6N background using standard CRISPR/Cas9 targeting (**Fig. S1**). CRISPR/Cas9-induced 127bp deletion in exon 3 results in a frame shift and subsequent introduction of a stop codon 32 codons downstream. ELANE KO (*Elane*$^{-/-}$) and Caspase-1/11 DKO mice were purchased from Jackson Laboratories (Bar Harbor, ME). Eight- to twelve-week-old mice were used in all experiments. Corresponding littermates were used as wild-type controls in all the experiments performed with KO mice. The Boston Children's Hospital Animal Care and Use Committee approved and monitored all procedures involving mice.

Cell lines

All cell lines were cultured at 37°C in a humidified atmosphere and 5% CO_2. Lenti-X 293T cells (Takara, Mountain View, CA) cells were maintained in Dulbecco's Modified Eagle Medium (DMEM) supplemented with 100 U/ml penicillin, 100 µg/ml streptomycin, and 10% fetal bovine serum (FBS) (Thermo Fisher Scientific, Waltham, MA). HL-60 cells were maintained in RPMI 1640 medium supplemented with 100 U/ml penicillin, 100 µg/ml streptomycin, and 10% FCS and differentiated into neutrophil-like cells with 1.25% dimethyl sulfoxide (in DMSO) for 6 days.

Plasmids

cDNA clones of human and mouse *GSDMD* were derived from KBM7 cells and mouse primary neutrophils, respectively. The genes were PCR amplified and inserted into pET SUMO (Thermo Fisher),

pCAG-MCS2-FOS (kindly provided by Dr. Morita), pLVX-TetOne (Takara), pCSII-EF-RfA, and pCSII-CMV-MCS-IRES2-Bsd (kindly provided by Dr. Miyoshi) vectors via sub-cloning. Site-directed mutagenesis was performed by overlap extension PCR using PrimeSTAR GXL DNA polymerase (Takara).

Hematologic analysis

Mice were anesthetized and immediately bled retro-orbitally into an EDTA-coated tube. Total cell counts were determined using a hemocytometer, and differential cell counts were performed using an automated hematology analyzer (Hemavet 850; Drew Scientific, Oxford, CT, or Sysmex, XT2000i). For BM cells, total cell counts were determined using a hemocytometer, and differential cell counts were conducted by microscopic analysis of Wright-Giemsa-stained cytospins or FACS analysis using a CANTOII flow cytometer with FACSDiva software (BD Biosciences, Franklin Lakes, NJ). The absolute number of neutrophils was then determined based on the cytospin or FACS analysis.

Human primary neutrophil isolation

Human primary neutrophils were isolated from apheresis-derived buffy coats provided by the Blood Bank Lab at the Boston Children's Hospital as previously described (Loison et al., 2014). All blood is drawn from healthy blood donors. All protocols have been approved by the Children's Hospital Institutional Review Board (IRB).

Preparation of highly purified neutrophils (HPNs)

To examine GSDMD and ELANE expression in neutrophils, we used highly purified neutrophils (HPNs). Traditional neutrophil isolation using Ficoll or Percoll gradients only reach ~95% purity, and contamination with other cell types (e.g., monocytes) is inevitable. Therefore, we purified neutrophils

from human blood using the traditional Ficoll method followed by negative selection to obtain HPNs (~99.5%). Briefly, human neutrophils were first prepared from apheresis-derived buffy coats using Ficoll as described above. The isolated neutrophils were further purified using the EasySep human neutrophil enrichment kit (StemCell Technologies, Cambridge, UK) according to the manufacturer's protocol. Neutrophil purity was determined by Wright-Giemsa staining.

Murine bone marrow neutrophil isolation

Murine bone marrow neutrophils were isolated from the femur and tibia as previously described (Subramanian et al., 2007). Briefly, bone marrow cells were collected from 8-14 weeks old mice and layered over discontinuous Percoll/HBSS gradients (52%, 64%, 76%) and centrifuged (1060g, 30 min, RT). The interface between the 64% and 76% layers containing neutrophils was harvested. Each preparation yielded about 7-11 million mature neutrophils (>85% purity).

Murine peripheral blood neutrophil isolation

8-14 weeks old mice were sacrificed by euthanizing with CO_2 and immediately bleed by cardiac puncture. The peripheral blood (1-2 ml) was then diluted with 3 ml HBSS with 15 mM EDTA. Cells were spun down (500g, 10 min, RT) and washed once with 4 ml HBSS with 15 mM EDTA. Red blood cells were lysed by resuspension in 5 ml ACK (Ammonium-Chloride-Potassium) Lysing Buffer (Thermo Fisher Scientific) for 5 min at RT. Lysis was stopped by addition of 15 ml RPMI+2% FBS followed by centrifugation at 400g for 5 min. After being washed with isolation buffer (2 mM EDTA, 1% endotoxin-free BSA in HBSS), the cells were resuspended in 6 ml 45% Percoll/HBSS, layered over two other discontinuous Percoll/HBSS gradients (3 ml 81% and 4.5 ml 62%), and centrifuged at 1500*g* at room temperature for 30 minutes (no brake, no acceleration). The interface between the 62% and 81% layers containing neutrophils was harvested and washed once with 10 ml of isolation buffer (1200g, 5

min). The purified neutrophils were resuspended in RPMI 1640 medium containing 10% heat-inactivated FBS and maintained at 37°C. Each preparation routinely yielded >1 million neutrophils (per mouse) with a purity of above 90% by Wright–Giemsa staining and FACS analysis with Gr-1 and CD11b monoclonal antibodies.

Neutrophil death analysis by FACS

Murine or human neutrophils were cultured in RPMI 1640 supplemented with 10 % heat-inactivated low endotoxin (≤ 5 EU/ml, usually ≤ 1 EU/ml) fetal calf serum (FCS, Gibco) and Penicillin-Streptomycin antibiotics at a density of 2×10^6 cells/ml at 37°C in a 5% CO_2 incubator. After indicated time periods, cells were then harvested, washed twice with ice cold PBS and stained with human Annexin V (FITC labeled, Invitrogen) and propidium iodide (PI) following a protocol provided by the manufacturer. FACS was performed using a CANTOII flow cytometer (Becton Dickinson, San Jose, CA). At least ten thousand events were recorded and analyzed using FlowJo software (Tree Star). In this FACS analysis, cell debris were eliminated by appropriate gating on forward and side scatter. Neutrophil death was assessed by the reduction of the percentage of $PI^-Annexin\ V^-$ viable cells ($\%PMN_{viable}$, relative to the input). At each time point (t^n), the total number of neutrophils ($PMN_{total\text{-}t^n}$), including both healthy and apoptotic cells, were counted using a hemocytometer. This number decreased gradually during neutrophil death, particularly at the later stage. The percentage of viable cells ($\%PMN_{viable\text{-}t^n}$) in this population was obtained by FACS analysis. The percentage of viable neutrophils relative to the input ($PMN_{total\text{-}t^0}$, total amount of cells at time "0") at each time point was calculated as follows: $\%PMN_{viable} = (PMN_{total\text{-}t^n} \times \%PMN_{viable\text{-}t^n}) / PMN_{total\text{-}t^0}$.

Mouse peritonitis model

$GSDMD^{-/-}$ or wild-type mice were intraperitoneally injected with $5x10^7$ *E.coli* (strain K12 BW25113) in 200 µl PBS. At indicate times after injection, the mice were sacrificed by euthanizing with CO_2.

Peritoneal exudate cells were then harvested by 3 successive washes with 10 ml HBSS containing 0.2% BSA and 20 mM EDTA. The exudate cell count (total cell number) was determined using a hemacytometer and the differential cell count was determined by FACS analysis. The cells were incubated with FITC anti-Gr1 antibody or anti-rat IgG antibody (as a control) for 15 min at room temperature. After being washed twice with PBS containing 2% BSA, the cells were analyzed by a BD FACSCanto II flow cytometer (BD Biosciences). Total number of neutrophils in the peritoneal exudates was then calculated accordingly as previously described (Bajrami et al., 2016). For measurement of cytokine levels in peritoneal cavity, peritoneal lavage fluids (PLF) were collected using 2 ml PBS/15 mM EDTA. Chemokine and cytokine levels in PLF were determined using ELISA kits.

Bacterial burden

Mouse peritonitis was induced as described above. Peritoneal lavage fluid (PLF) was collected by 3 successive washes with 10 ml HBSS containing 0.2% BSA and 20 mM EDTA. PLFs were then serially diluted in ice-cold sterile PBS, and aliquots were spread on Luria broth (LB) agar plates. After overnight incubation at 37°C, colonies were counted, and bacterial viability was expressed as colony-forming units (cfu) in total lavage fluid.

TG induced neutrophil recruitment to flamed peritoneal cavity

Peritonitis was induced by intraperitoneal injection of 3% thioglycollate (TG) solution as previously described (Jia et al., 2007). Peritoneal lavage fluids were collected from wild-type and GSDMD knockout mice by 3 successive washes with 10 ml HBSS containing 0.2% BSA and 20 mM EDTA, 7 hr after TG injection. The exudate cell count (total cell number) was determined using a hemacytometer and the differential cell count was determined by FACS analysis. The cells were incubated with FITC anti-Gr1 antibody for 15 min at room temperature. After being washed twice with PBS containing 2%

BSA, the cells were analyzed by a BD FACSCanto II flow cytometer (BD Biosciences). Total number of neutrophils in the peritoneal exudates was then calculated accordingly.

In vitro bactericidal assay

Live *E. coli* particles (ATCC 19138; American Type Culture Collection, 5×10^5 cfu) were opsonized with mouse serum (final concentration 10%) at 37°C for 30 min and then incubated with neutrophils (1×10^5 cells/reaction for bone marrow neutrophils and 1×10^4 cells/reaction for peripheral blood neutrophils) in HBSS (without mouse serum) at 37°C for the indicated times. Samples were then serially diluted and spread on LB agar plates. The number of live *E. coli* cells in each sample was determined after overnight incubation at 37°C. Neutrophil intracellular bactericidal activity was measured using an antibiotic protection assay. Briefly, mouse neutrophils (10^6 cells for bone marrow neutrophils and 1×10^5 cells for peripheral blood neutrophils) were incubated with serum-opsonized live *E. coli* particles at a ratio of 1:5 and incubated at 37°C for 1 h. Kanamycin was then added at the final concentration of 50 μg/ml to kill extracellular bacteria. After an additional 15 min incubation, cells were washed twice with HBSS and lysed with 1 ml sterile water at room temperature. Samples were serially diluted and spread on LB agar plates. Colonies were counted after overnight incubation at 37°C.

In vitro Phagocytosis assay

Fluorescein-conjugated Phrodo™ Green *E.coli* bioparticles (Invitrogen) were reconstituted in HBSS and opsonized with 12.5% mouse serum at 37°C for 30 min. Mouse bone marrow neutrophils were incubated with serum-opsonized bioparticles at a ratio of 1:10 (neutrophils : bioparticles), and incubated at 37°C for 1 hour. Negative controls were incubated on ice for 1 hour. The assays were terminated by cooling the cells on ice. The number of internalized particles was counted under a fluorescence microscope (Olympus lX17, 100X objective). Phagocytosis index was expressed as the number of the

internalized particles per 100 neutrophils. Phagocytosis efficiency was expressed as the percentage of neutrophils that engulfed at least one bioparticle. More than 200 cells were counted from random fields per coverslip for each group.

Recombinant protein expression

Human and mouse pET SUMO-GSDMD plasmids were transformed into BL21(DE3) competent cells for protein overexpression. *E. coli* organisms were pre-cultured in 2 ml LB medium containing 50μg/ml kanamycin at 37ºC overnight. 2 ml bacteria culture was then transferred into 300 ml LB medium containing 50 μg/ml kanamycin and further cultured at 37ºC to an OD 600 of 0.5-0.8. Subsequently, isopropyl β-D-1-thiogalactopyranoside (IPTG) at a final concentration of 1mM was added to the culture medium to induce protein expression. *E. coli* cultures were further incubated at 25ºC overnight. Cells were collected by centrifugation at 5000 rpm for 10 min and stored at -80°C. 6xHis-SUMO fusion GSDMD protein purification was carried out under native conditions using a Ni-NTA Fast Start kit (Qiagen, Limburg, NL). Following elution from the Ni-NTA affinity column with native elution buffer, the proteins were dialyzed in PBS overnight at 4ºC and stored at -80ºC.

Preparation of neutrophil lysate

Purified neutrophils were washed once with ice cold PBS then incubated for 30 min on ice in Triton lysis buffer (20 mM Tris-HCl (pH 7.4), 135 mM NaCl, 1% Triton X-100, 10% glycerol). Samples were centrifuged at 14,000 rpm for 30 min at 4°C. The supernatant was collected and stored at -80°C.

In-gel digestion and LC/MS/MS analysis

N-terminal His-tagged recombinant GSDMD (20 μg) was incubated with recombinant ELANE or neutrophil lysate (7 μg of protein) at 37 °C for 1 h. His-tagged proteins were then enriched by precipitation using Ni-NTA beads in the presence of DFP (100 μM). After three washes, His-tagged proteins were eluted using imidazole and resolved by SDS-PAGE. In-gel digestion was performed manually in 96-well plate format. Gel bands were first cut and diced into ~1mm cubes and transferred into the wells before being de-stained with 50/50 acetonitrile/50mM NH_4HCO_3 solution, dithiothritol (DTT)-reduced and iodoacetamide (IAM)-alkylated, followed by trypsin or AspN digestion overnight at 37°C. Peptides were extracted into 40/60 acetonitrile/0.1% formic acid solution and dried in a SpeedVac. The dry peptide extract was reconstituted in 22 μL 2%/0.2% acetonitrile/formic acid solution and analyzed on a 1D nanoLC-MS/MS platform using a standardized 110 min method (Mass Spec Facility, Broad Institute, MA). Peptides were separated on a C18-AQ column (75 μm × 50 cm, Reprosil-Pur C18-AQ, 1.9 μm) at 275 nl/min and analyzed on a QExactive Plus mass spectrometer in data-dependent acquisition (DDA) mode with MS1 at 35000 and MS2 at 17500 resolution, respectively.

Database search

MS data were first QC checked using in-house developed software (Mass Spec Facility, Broad Institute) and subsequently searched against the modified Swiss-Prot human database using Andromeda integrated into MaxQuant with mass tolerance of 20 ppm (MS1) and 4.5 ppm (MS2). The modified Swiss-Prot human database includes all Gasdermin-D protein sequences derived by sequential C-terminal amino acid removal. Protein identification and concentration were directly reported from MaxQuant and then further processed using an in-house developed pipeline for protein identification and quantitation.

Western blotting

Neutrophils (4 million cells/data point) were centrifuged and lysed immediately with 100 µl boiling protein loading buffer containing protease inhibitor cocktail (Invitrogen, Carlsbad, CA) and DFP (2mM). Samples were incubated at 100ºC for 5 min and transferred to ice. After brief sonication (5-10 s), 25 µl of cell lysate was subjected to 5-20% gradient SDS-PAGE. Proteins were transferred to polyvinylidene difluoride membranes (Millipore, Bedford, MA). After blocking the membranes in TBS containing 5% BSA (Sigma) and 0.02% Triton X-100 for 1 h, primary antibodies were added in blocking solution at the following dilutions: mouse anti-GSDMD antibody (Abnova, Taiwan, 1:1000), anti-Caspase-1 (Adipogen, San Diego, CA, 1:1000), anti-human and mouse ELA2 antibodies (R&D Systems, Minneapolis, MN, 1:1000), mouse anti-actin and FLAG antibodies (Sigma, 1:2000). Primary antibody incubations were at 4°C overnight. After washing, goat HRP-conjugated secondary antibodies (Santa Cruz Biotechnology Inc., Dallas, TX) were added (1:10,000) in blocking solution and the membrane incubated at RT for 1 h. The immunocomplexes were detected with Super Signal West Femto substrate (Pierce, Rockford, IL) using an ImageQuant LAS-4000 (GE, Fairfield, CT). Densitometry was performed using ImageJ software Gel Analyzer plug-in (Luo et al., 2002).

Neutrophil elastase activity assay

The ELANE chromogenic substrate MeOSuc-Ala-Ala-Pro-Val-pNA was purchased from Santa Cruz Biotechnology Inc. Cleavage of p-nitroaniline (pNA) from the substrate by ELANE increases absorbance at 405 nm. For mouse ELANE activity, recombinant ELANE (0.1 µg) was incubated with the substrate (500 µM) in 100 ul of MES reaction buffer (50 mM MES pH 5.5, 50 mM NaCl) at 37ºC for 60 min. For human ELANE activity, the indicated amount of recombinant ELANE was incubated with the substrate (500 µM) in 100 ul of PBS at 37ºC for 30 min. Cleavage of the substrate product was detected at OD 405 in a 96-well microplate reader.

Lactate dehydrogenase (LDH) cytotoxicity assay

LDH release was assayed using the CytoTox 96® Non-Radioactive Cytotoxicity Assay (Promega, Madison, WI) following the manufacturer's protocol. HEK293T cells were transfected with indicated GSDMD expressing constructs and then incubated at 37ºC for 24 h. The culture media were collected and centrifuged at 400 x g for 5 min to remove cell debris. LDH release in the media was measured at OD 490. The relative LDH release was expressed as the percentage LDH activity in supernatants of cultured cells (medium) compared with total LDH (from media and the cells) and used as an index of cytotoxicity.

Lysosomal Membrane Permeabilization (LMP) assay

Human neutrophils were isolated as described above and cultured for indicated times. Lysosomal membrane permeability was then assayed as previously described (Loison et al., 2014). Briefly, cells were stained with Acridine Orange (2 ug/ml) in RPMI plus 10 % FCS for 15 min at 37ºC and then washed once in PBS. The red fluorescence was measured by FACS in the PercP/Cy5 channel. The percentages of pale (AO negative) cells were quantified and normalized to the percentage of the control (untreated) cells.

Preparation of neutrophil cytosolic fraction

Purified neutrophils were washed once with ice cold PBS then incubated for 30 min on ice in hypotonic buffer (20 mM HEPES-KOH, pH 7.5, 10 mM KCl, 1.5 mM $MgCl_2$, 1 mM sodium EDTA, 1 mM DTT) supplemented with protease inhibitor cocktail (Roche, Basel, Switzerland). Cells were then lysed by 20-30 strokes of a Dounce homogenizer with pestle B. Extracts were then centrifuged at 16,000 x g at 4°C for 30 min. Supernatants were collected as cytosolic fractions.

Immunofluorescent staining

For immunostaining of GSDMD, HEK293T cells were plated onto 18 mm diameter, #1.5 thickness glass coverslips (NeuVitro Corp., El Monte, CA) in 6-well plates overnight. Cells were transfected with 1ug of indicated 3xFLAG-tagged GSDMDs and incubated for 24 h. Cells were fixed for 30 min in 3% paraformaldehyde (PFA) before being washed three times with PBS and permeabilized for 15 min with 0.25% saponin in PBS. Blocking was performed with 2% BSA in PBS for 30 min at RT. The diluted primary anti-FLAG antibodies (1:2000) were added and incubated overnight at 4°C. After three washes with PBS, the Alexa fluor 594 dye-conjugated secondary antibody (1:1000) was added and incubated for 1 h at room temperature. Staining was visualized using the Olympus Fluoview FV1000 confocal system and images were taken using a 60x objective lens.

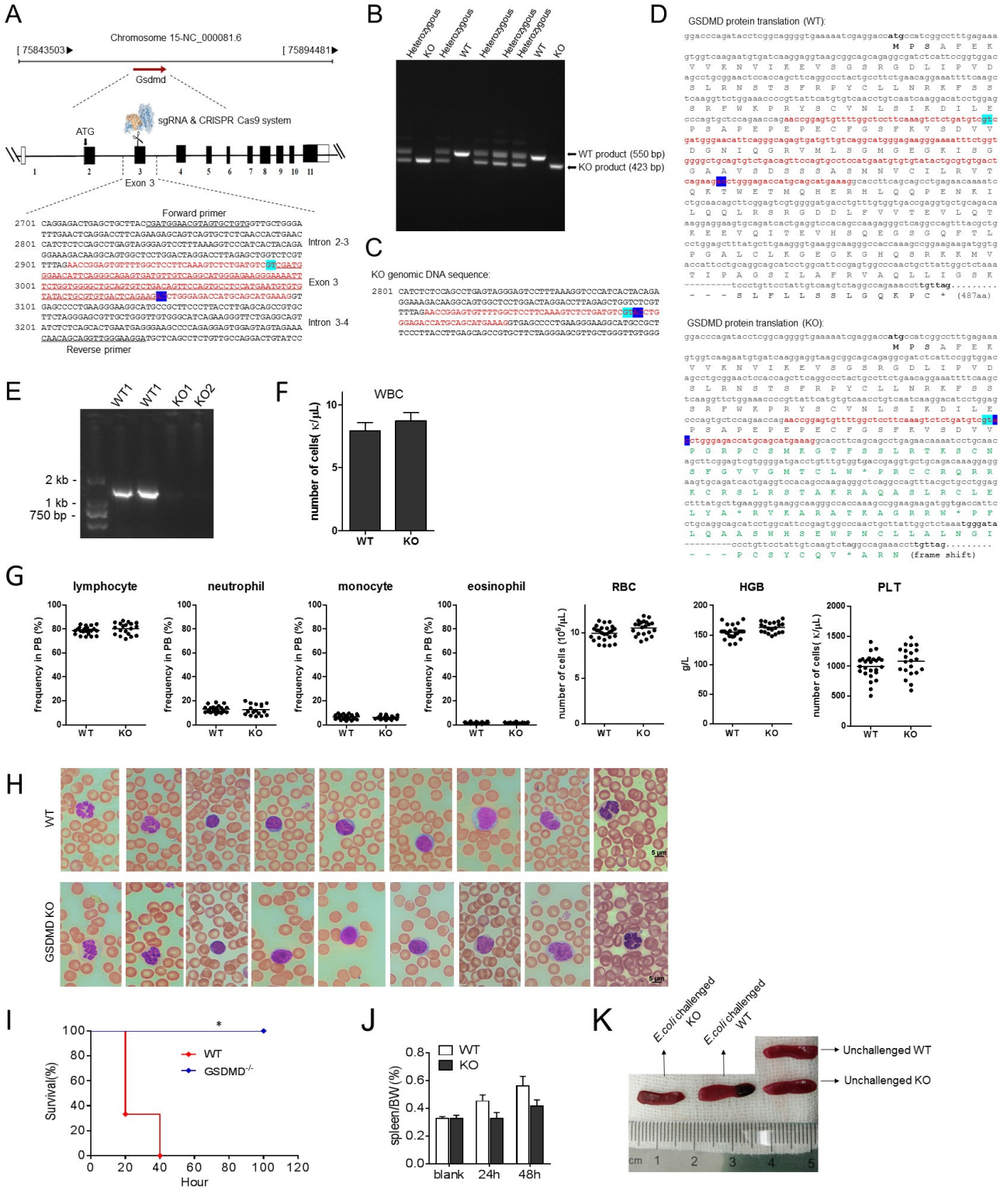
A
Chromosome 15-NC_000081.6
[75843503▶
[75894481▶
Gsdmd
sgRNA & CRISPR Cas9 system
ATG
1 2 3 4 5 6 7 8 9 10 11
Exon 3
Forward primer
Intron 2-3
Exon 3
Intron 3-4
Reverse primer
B
Heterozygous KO
Heterozygous WT
Heterozygous WT
Heterozygous KO
WT product (550 bp)
KO product (423 bp)
C
KO genomic DNA sequence:
D
GSDMD protein translation (WT):
(487aa)
GSDMD protein translation (KO):
(frame shift)
E
WT1 WT1 KO1 KO2
2 kb -
1 kb -
750 bp -
F
WBC
number of cells(K/μL)
WT KO
G
lymphocyte
neutrophil
monocyte
eosinophil
RBC
HGB
PLT
frequency in PB (%)
number of cells (10^6/μL)
g/L
number of cells(K/μL)
WT KO
H
WT
GSDMD KO
5 μm
I
Survival(%)
WT
GSDMD-/-
Hour
J
spleen/BW (%)
WT
KO
blank 24h 48h
K
E.coli challenged KO
E.coli challenged WT
Unchallenged WT
Unchallenged KO
cm 1 2 3 4 5

Figure S1. Related to Figure 1. Generation of *Gsdmd*-deficient mice using the CRISPR/Cas9 system. **(A)** Schematic of the targeting strategy. Mouse *Gsdmd* gene structure and the location of exon 3 are shown. The sequence deleted in the KO mouse is underlined. The forward and reverse primers used for genotyping are indicated. **(B)** Genome PCR analysis in wild-type (WT), heterozygous, and homozygous (KO) mutant mice using forward and reverse primers. **(C)** Genomic DNA sequence of *Gsdmd*-deficient mice. The desired deletion of the *Gsdmd* gene was confirmed. **(D)** CRISPR/Cas9-induced 127 bp deletion results in a frame shift in exon 3 and subsequent introduction of a stop codon 32 codons downstream. **(E)** Complete depletion of *Gsdmd* mRNA in the KO mice was confirmed by qPCR. **(F)** Total white blood cell count (WBC) in wild-type (WT) and *Gsdmd*-deficient (KO) mice (n >15 mice per genotype). No significant difference ($P < 0.05$) was found between groups. **(G)** Differential white blood cell counts, red blood cell (RBC) counts, platelets (PLT) counts, and hemoglobin (HGB) levels in WT and KO mice (n >15 mice per genotype). No significant difference ($P < 0.05$) was found between groups. **(H)** Peripheral blood smears from WT and KO mice. Shown are representative images. **(I)** Survival rates of mice challenged with lethal sepsis. Age and sex matched (9-week old, n=6) mice were challenged with 30 mg/kg LPS (E.coli 0111:B4). Survival rates were analyzed using the Kaplan-Meier survival curves and log-rank test. * $P < 0.05$ *vs* WT. **(J)** Relative ratio of spleen weight vs. body weight following *E. coli* challenge. The overall weight of each mouse was similar, so correction of spleen weight by body weight did not affect the conclusions. Values are mean ± SD. *$P < 0.01$ (Student's t-test). **(K)** Picture of spleens from unchallenged and *E. coli* challenged WT and KO mice. Experiments were conducted as described in **Fig 1A**.

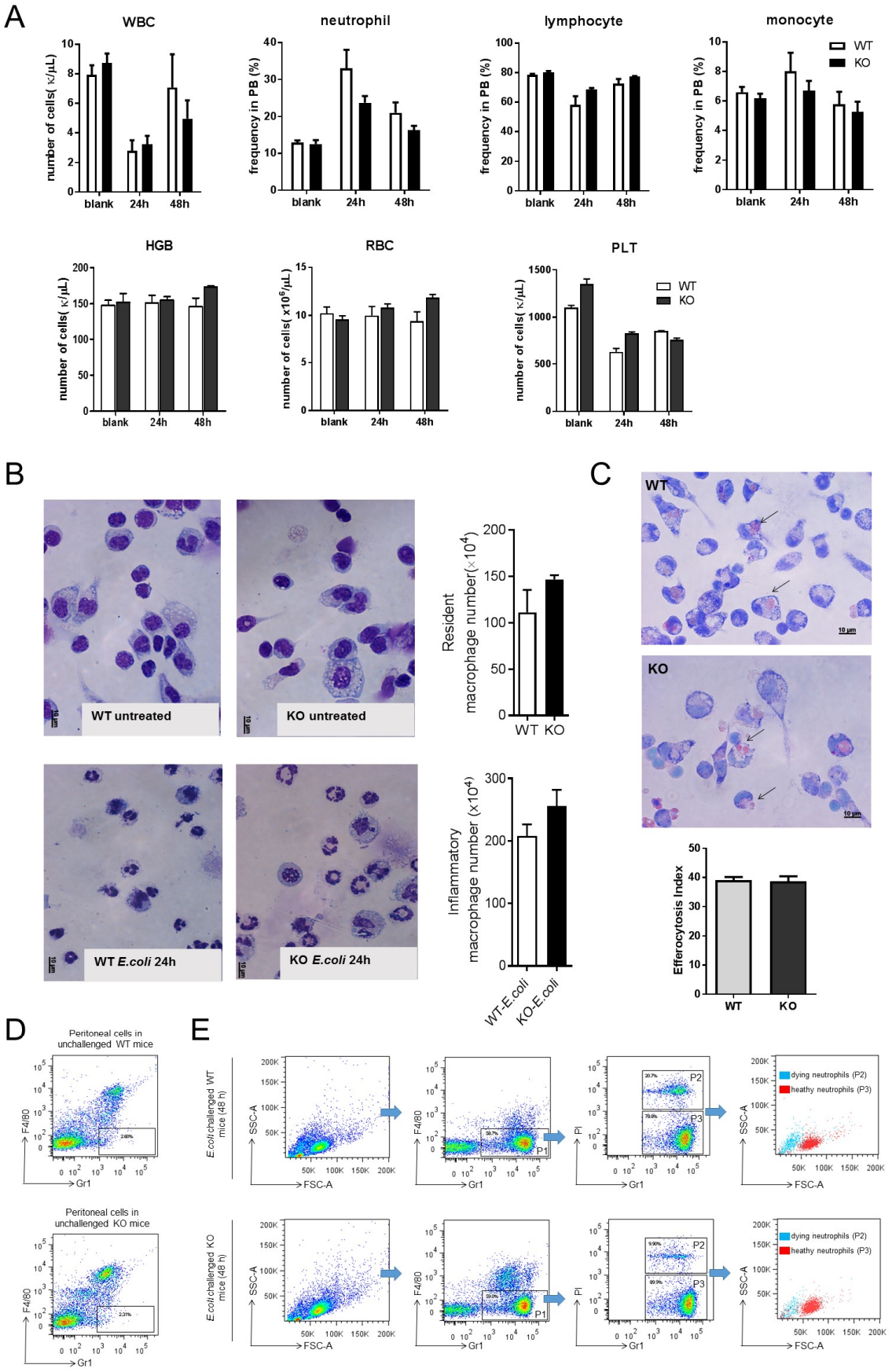
A
WBC
neutrophil
lymphocyte
monocyte
HGB
RBC
PLT
number of cells(κ/μL)
frequency in PB (%)
number of cells(x10^6/μL)
blank
24h
48h
WT
KO
B
WT untreated
KO untreated
WT E.coli 24h
KO E.coli 24h
Resident macrophage number(×10^4)
Inflammatory macrophage number (×10^4)
WT-E.coli
KO-E.coli
C
WT
KO
Efferocytosis Index
D
Peritoneal cells in unchallenged WT mice
Peritoneal cells in unchallenged KO mice
F4/80
Gr1
E
E.coli challenged WT mice (48 h)
E.coli challenged KO mice (48 h)
SSC-A
FSC-A
PI
P1
P2
P3
dying neutrophils (P2)
heathy neutrophils (P3)

Figure S2. Related to Figure 3. The elevated neutrophil accumulation in GSDMD-deficient mice was due to delayed neutrophil death. (A) Total white blood cell count (WBC), differential white blood cell counts, red blood cell (RBC) counts, platelets (PLT) counts, and hemoglobin (HGB) levels in wild-type (WT) and *Gsdmd*-deficient (KO) mice (male, 8-12 week old) after *E.coli* challenge. The experiments were conducted as described in **Fig. 2E**. No significant difference ($P < 0.05$) was found between groups. (**B**) The numbers of resident and inflammatory macrophages in the peritoneal cavity in WT and *Gsdmd*-deficient (KO) mice. The macrophages were identified by morphology examination of Wright-Giemsa stained peritoneal cells (large size, large cytoplasmic region, and single, round nucleus). All values represent mean ± SD of three independent experiments. **(C)** Clearance of dead neutrophils by macrophages (efferocytosis). The assay was conducted as previously described (Mondal et al., 2011). Briefly, wild-type or *Gsdmd*-deficient (KO) peritoneal macrophages were incubated with one-day cultured bone marrow neutrophils at a density of (1:10) for 90 minutes at 37°C. Cells were washed and efferocytosis was analyzed by HEMA3 staining. Number of macrophages containing one or more apoptotic cell was scored as % efferocytosis. Arrowheads indicate macrophage containing engulfed apoptotic cells. All values represent mean ± SD of three independent experiments. **(D)** Representative flow cytometry plots for peritoneal neutrophils in unchallenged WT and *Gsdmd*-deficient (KO) mice. Numbers denote the frequency of each population among live singlets. Very few neutrophils were detected in the peritoneal cavity of WT or KO mice. (**E**) Gating strategy to analyze neutrophil death in inflamed peritoneal cavities in WT and KO mice. The experiments were conducted as described in **Fig. 3C**.

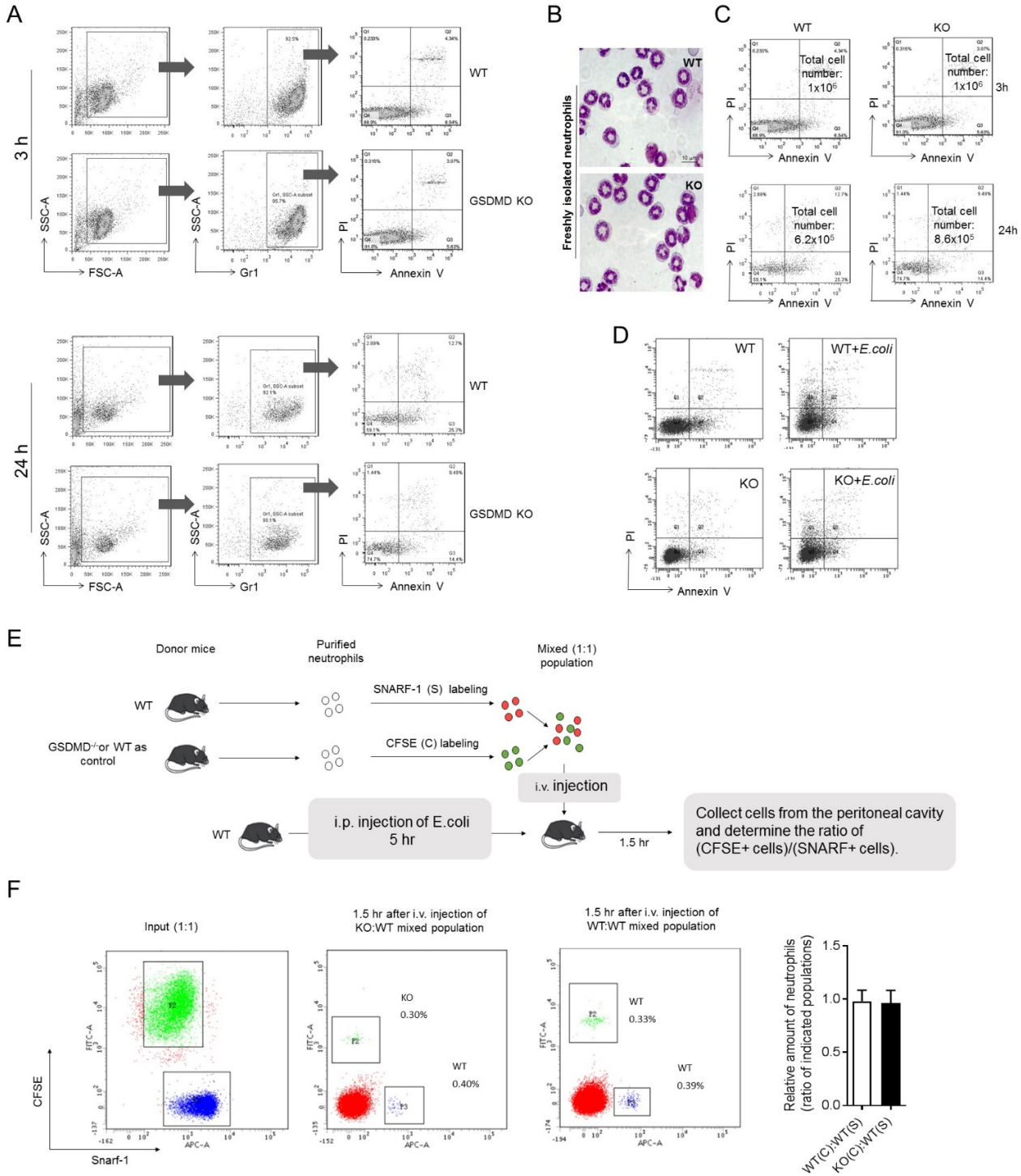
A
3 h
SSC-A
FSC-A
Gr1
PI
Annexin V
WT
GSDMD KO
24 h
B
Freshly isolated neutrophils
WT
KO
C
WT
KO
Total cell number: 1x10^6
Total cell number: 6.2x10^5
Total cell number: 8.6x10^5
3h
24h
PI
Annexin V
D
WT
WT+E.coli
KO
KO+E.coli
E
Donor mice
Purified neutrophils
Mixed (1:1) population
WT
GSDMD-/- or WT as control
SNARF-1 (S) labeling
CFSE (C) labeling
i.v. injection
i.p. injection of E.coli 5 hr
1.5 hr
Collect cells from the peritoneal cavity and determine the ratio of (CFSE+ cells)/(SNARF+ cells).
F
Input (1:1)
1.5 hr after i.v. injection of KO:WT mixed population
1.5 hr after i.v. injection of WT:WT mixed population
CFSE
Snarf-1
FITC-A
APC-A
KO
0.30%
WT
0.40%
WT
0.33%
WT
0.39%
Relative amount of neutrophils (ratio of indicated populations)
1.5
1.0
0.5
0.0
WT(C):WT(S)
KO(C):WT(S)

Figure S3. Related to Figure 3. The role of GSDMD in regulating neutrophil death and recruitment. (A) Gating strategy to analyze the death of *in vitro* cultured WT and *Gsdmd*-deficient (KO) neutrophils. In this FACS-based analysis, the characteristic phosphatidylserine exteriorization was detected by annexin V, an anticoagulant protein that has high affinity and selectivity for phosphatidylserine. The membrane integrity of the dying neutrophils was monitored using propidium iodide (PI), a membrane impermeable dye. Experiments were conducted as described in **Fig 3E**. **(B)** Freshly isolated WT and GSDMD-deficient neutrophils. Shown are representative images. **(C)** Death of *in vitro* cultured WT and GSDMD-deficient neutrophils. Neutrophils were cultured in RPMI 1640 medium containing 10% heat-inactivated FBS at a density of 2 x 10^6 cells per ml. Dying cells were detected by annexin V-FITC and propidium iodide (PI) staining. *Shown are representative FACS* plots depicting healthy (PI^-/annexin V^-) and dying (PI^+ or annexin V^+) peritoneal neutrophils. Experiments were conducted as described in **Fig 3E**. **(D)** Death of *in vitro* cultured WT and GSDMD-deficient neutrophils in the presence of *E.coli.* Neutrophils were cultured with *E.coli* (1:5 ratio) for 2 hours. *Shown are representative FACS* plots depicting healthy (PI^-/annexin V^-) and dying (PI^+ or/and annexin V^+) neutrophils. Experiments were conducted as described in **Fig 3G. (E-F)** Disruption of GSDMD in neutrophils did not affect neutrophil recruitment during infection and inflammation. **(E)** Recruitment of adoptively transferred neutrophils. WT and GSDMD deficient neutrophils were labeled with intracellular fluorescent dye intracellular fluorescent dye 5-(and -6)-carboxyfluorescein diacetate succinimidyl esters (CFSE) or 5-(and -6)-chloromethyl SNARF-1 acetate (SNARF-1). Labeled cells were mixed (1:1) and intravenously injected to WT mice challenged with 3% thioglycollate (TG). The cells accumulated in the peritoneal cavity were collected at indicated time point and analyzed using a FACSCanto II flow cytometer. **(F)** The ratios of adoptively transferred WT and GSDMD-deficient neutrophils. All values represent mean ± SD of three experiments.

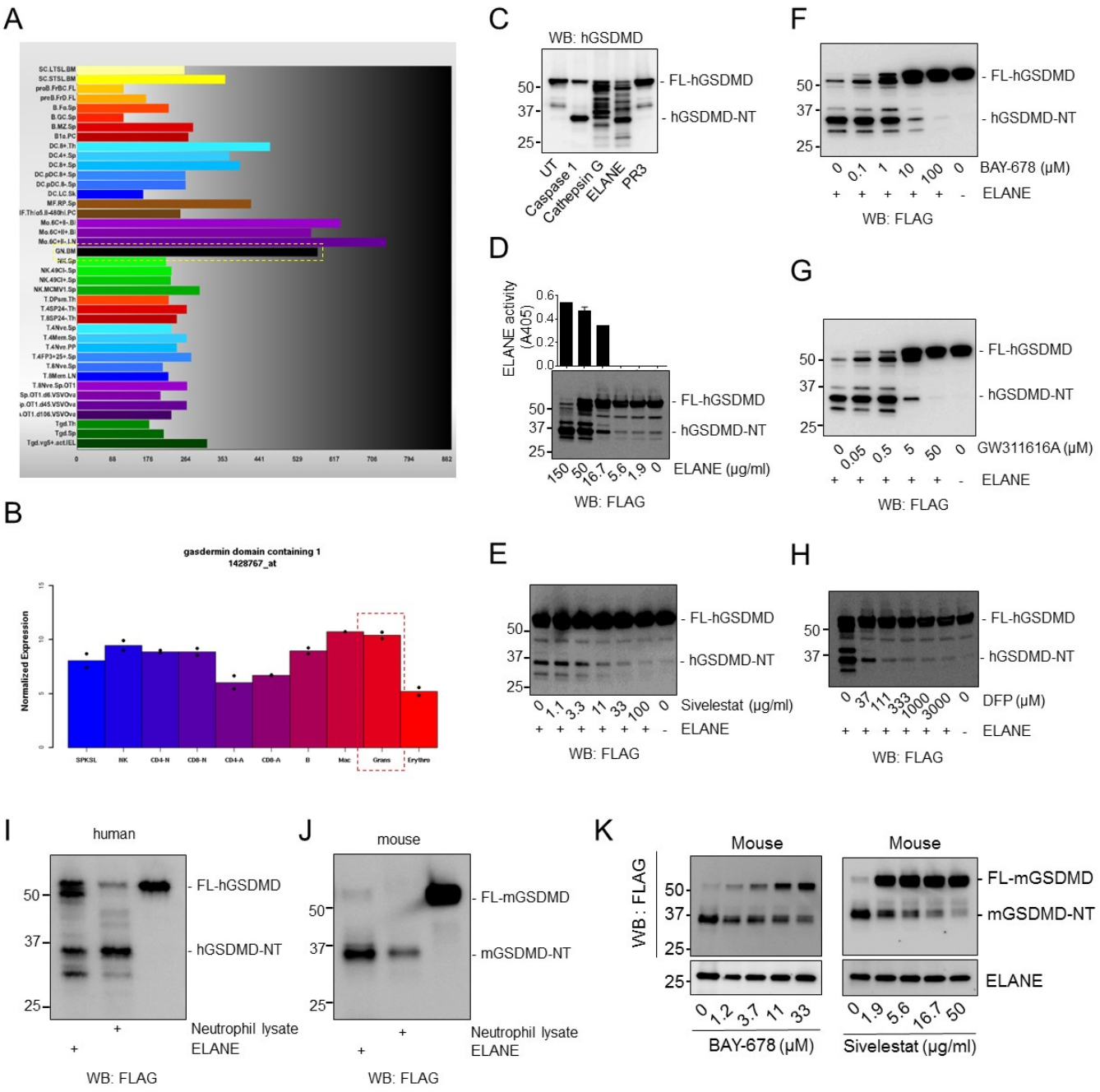
A
B
gasdermin domain containing 1
1428767_at
Normalized Expression
SPKSL
NK
CD4-N
CD8-N
CD4-A
CD8-A
B
Mac
Grans
Erythro
C
WB: hGSDMD
FL-hGSDMD
hGSDMD-NT
UT
Caspase 1
Cathepsin G
ELANE
PR3
D
ELANE activity (A405)
ELANE (µg/ml)
WB: FLAG
E
Sivelestat (µg/ml)
ELANE
WB: FLAG
F
BAY-678 (µM)
ELANE
WB: FLAG
G
GW311616A (µM)
ELANE
WB: FLAG
H
DFP (µM)
ELANE
WB: FLAG
I
human
FL-hGSDMD
hGSDMD-NT
Neutrophil lysate
ELANE
WB: FLAG
J
mouse
FL-mGSDMD
mGSDMD-NT
Neutrophil lysate
ELANE
WB: FLAG
K
Mouse
Mouse
WB : FLAG
FL-mGSDMD
mGSDMD-NT
ELANE
BAY-678 (µM)
Sivelestat (µg/ml)

Figure S4. Related to Figure 4. GSDMD cleavage in neutrophils is mediated by ELANE. **(A)** GSDMD mRNA expression in hematopoietic cells from the ImmGen Database. BM neutrophil population is highlighted in yellow. **(B)** GSDMD mRNA expression in hematopoietic cells from the Gene Expression Across Multiple Hematopoietic Lineages Database. Neutrophil population is highlighted in red. **(C-H)** ELANE-mediated cleavage of human GSDMD. **(C)** FLAG-hGSDMD was overexpressed in HEK293T cells. Cell lysates containing recombinant FLAG-hGSDMD were incubated with recombinant human caspase 1 (100 units), PR3 (2 μg), ELANE (2 μg), or cathepsin G (2 μg) at 37°C for 30 min in a 6-well plate. The protein samples were subjected to SDS-PAGE followed by western blotting with an anti-GSDMD antibody. The positions of the full-length (FL-hGSDMD) and ELANE-cleaved N-terminal hGSDMD (hGSDMD-NT) are indicated. **(D)** The degree of GSDMD cleavage was positively correlated with the amount of ELANE enzymatic activity in the reaction. FLAG-hGSDMD was incubated with different doses of ELANE. ELANE enzymatic activity was determined using an ELANE-specific substrate following the manufacturer's protocol. **(E)** ELANE-mediated GSDMD cleavage conducted in the presence of indicated amount of sivelestat. **(F)** ELANE-mediated GSDMD cleavage conducted in the presence of indicated amount of BAY-678. **(G)** ELANE-mediated GSDMD cleavage conducted in the presence of indicated amount of GW311616A. **(H)** ELANE-mediated GSDMD cleavage conducted in the presence of indicated amount of pan-serine protease inhibitor DFP. **(I-J)** GSDMD N-terminal fragment produced by neutrophil lysate was the same size as the one cleaved by recombinant ELANE. **(I)** Cleavage of human GSDMD. **(J)** Cleavage of mouse GSDMD. The positions of the full-length and ELANE-cleaved GSDMD are indicated. **(K)** Mouse GSDMD cleavage by neutrophil lysate was inhibited by ELANE-specific protease inhibitors in a dose dependent manner. FLAG-mGSDMD was overexpressed in HEK293T cells. Cell lysates containing recombinant FLAG-hGSDMD were incubated with mouse neutrophil lysate in the presence of indicated amount of ELANE inhibitors BAY-678 or sivelestat at 37°C for 30 min. The full-length and ELANE-cleaved GSDMD were detected with an anti-FLAG antibody.

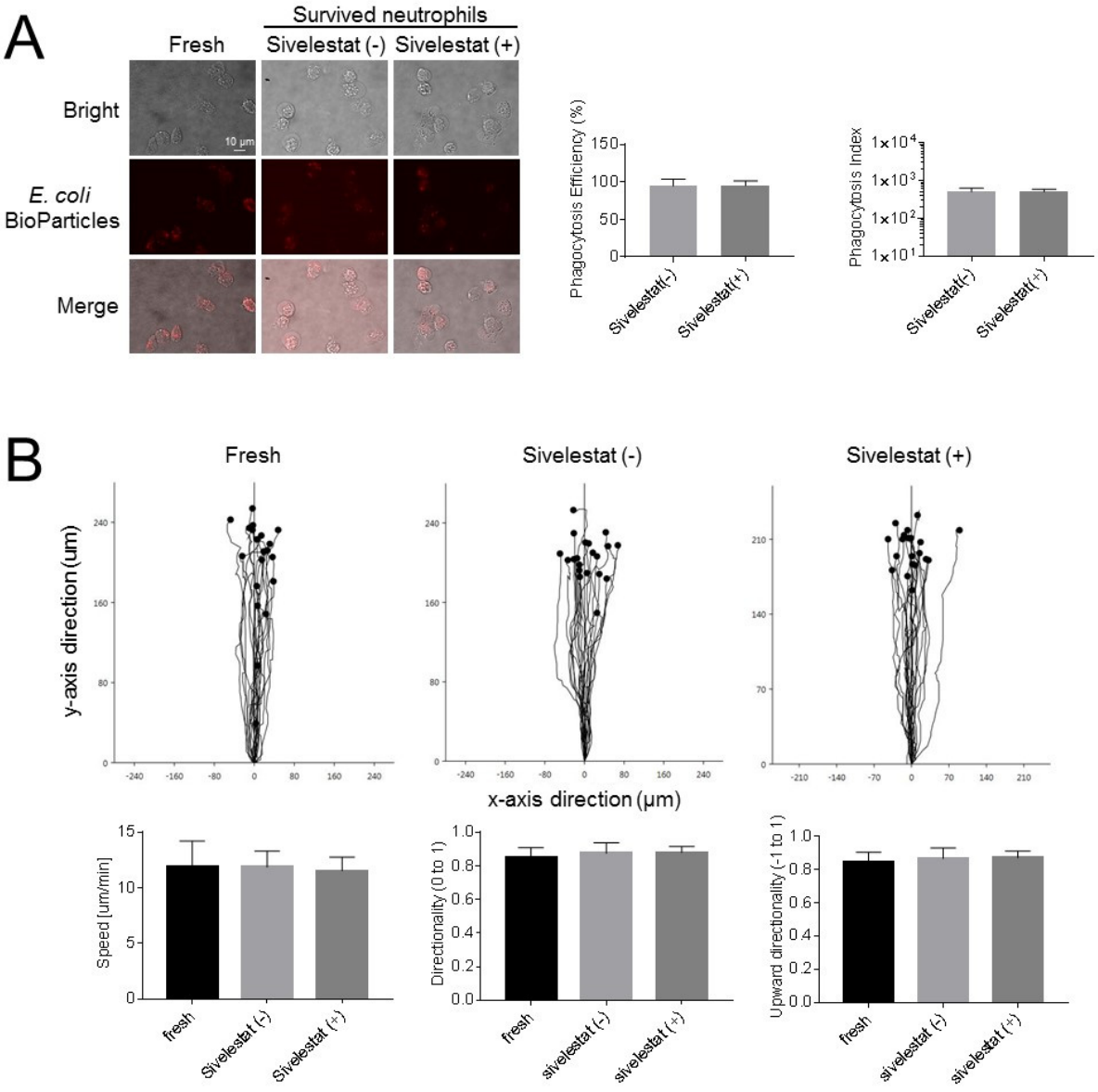

Figure S5. Related to Figure 5. Chemotaxis and phagocytosis capability of the survived cells. (A) *In vitro* phagocytosis assay. Human neutrophils were cultured in the presence or absence of Sivelestat (1μg/ml) for 24 hr. Fluorescein-conjugated *E. coli* bioparticles (10 μg/ml) were opsonized with 20% human serum and incubated with survived neutrophils at 37°C for 90 min. Cells were fixed with 4% PFA and phagocytosed bioparticles were manually counted to determine phagocytosis efficiency and index. **(B)** Neutrophil chemotaxis assay. Neutrophil chemotaxis was assessed using EZ-Taxiscan chemotaxis device (Effector Cell Institute, Tokyo, Japan) as previously described (Hattori et al., 2010; Sakai et al., 2012). Chemotaxis was triggered by fMLP (1 μl of 0.1 μM human fMLP, Sigma: F3506). Chemotaxis speed, directionality and upward directionality were calculated using Gradientech Tracking Tool™ PRO v2.1. All values represent mean ± SD (n=20 cells).

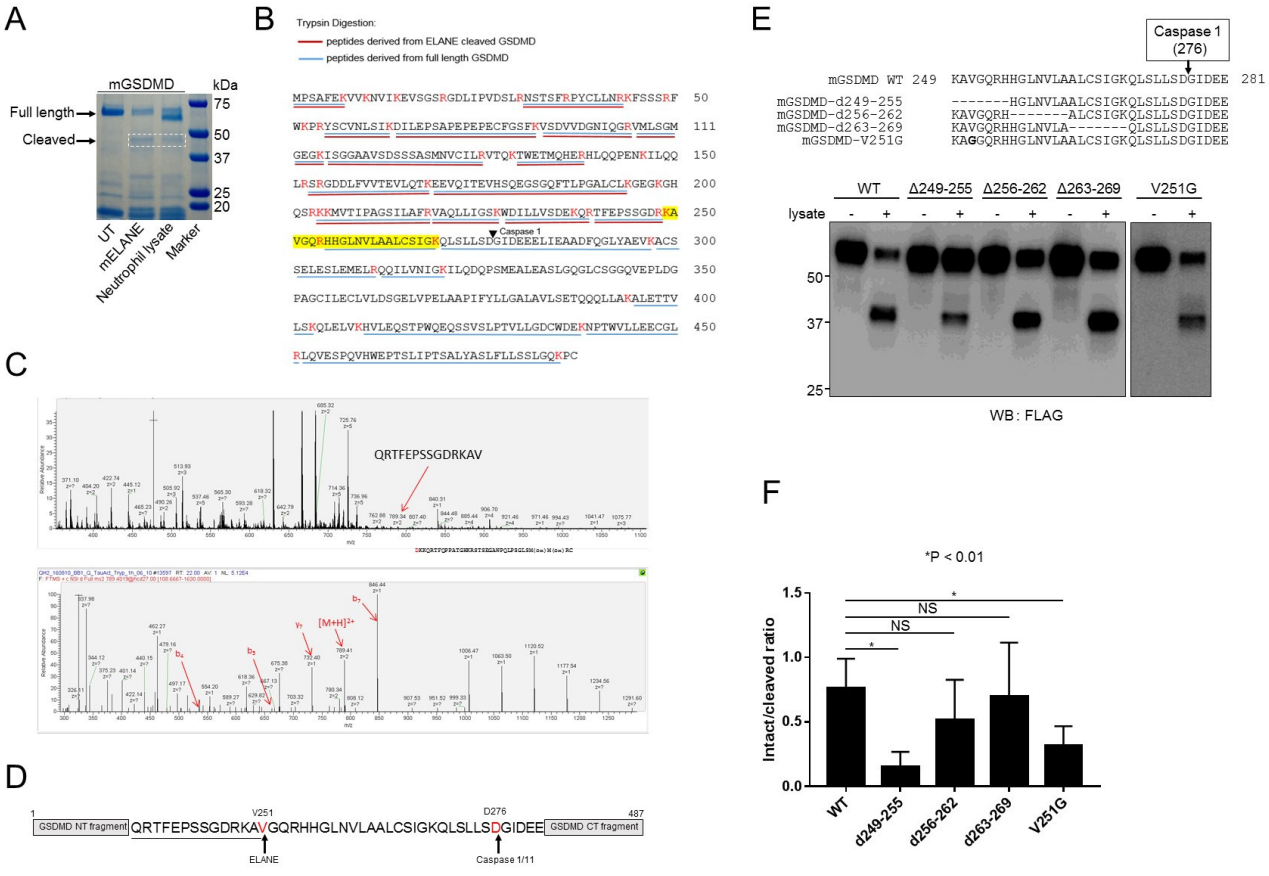
A
mGSDMD
kDa
Full length
Cleaved
75
50
37
25
20
UT
mELANE
Neutrophil lysate
Marker
B
Trypsin Digestion:
peptides derived from ELANE cleaved GSDMD
peptides derived from full length GSDMD
MPSAFEKVVKNVIKEVSGSRGDLIPVDSLRNSTSFRPYCLLNRKFSSSRF 50
WKPRYSCVNLSIKDILEPSAPEPEPECFGSFKVSDVVDGNIQGRVMLSGM 111
GEGKISGGAAVSDSSSASMNVCILRVTQKTWETMQHERHLQQPENKILQQ 150
LRSRGDDLFVVTEVLQTKEEVQITEVHSQEGSGQFTLPGALCLKGEGKGH 200
QSRKKMVTIPAGSILAFRVAQLLIGSKWDILLVSDEKQRTFEPSSGDRKA 250
VGQRHHGLNVLAALCSIGKQLSLLSDGIDEEELIEAADFQGLYAEVKACS 300
SELESLEMELRQQILVNIGKILQDQPSMEALEASLGQGLCSGGQVEPLDG 350
PAGCILECLVLDSGELVPELAAPIFYLLGALAVLSETQQQLLAKALETTV 400
LSKQLELVKHVLEQSTPWQEQSSVSLPTVLLGDCWDEKNPTWVLLEECGL 450
RLQVESPQVHWEPTSLIPTSALYASLFLLSSLGQKPC
Caspase 1
C
QRTFEPSSGDRKAV
D
1
GSDMD NT fragment
QRTFEPSSGDRKAVGQRHHGLNVLAALCSIGKQLSLLSDGIDEE
GSDMD CT fragment
487
V251
D276
ELANE
Caspase 1/11
E
Caspase 1
(276)
mGSDMD WT 249 KAVGQRHHGLNVLAALCSIGKQLSLLSDGIDEE 281
mGSDMD-d249-255 -------HGLNVLAALCSIGKQLSLLSDGIDEE
mGSDMD-d256-262 KAVGQRH-------ALCSIGKQLSLLSDGIDEE
mGSDMD-d263-269 KAVGQRHHGLNVLA-------QLSLLSDGIDEE
mGSDMD-V251G KAGGQRHHGLNVLAALCSIGKQLSLLSDGIDEE
WT
Δ249-255
Δ256-262
Δ263-269
V251G
lysate
- + - + - + - + - +
50
37
25
WB: FLAG
F
*P < 0.01
Intact/cleaved ratio
1.5
1.0
0.5
0.0
NS
NS
*
*
WT
d249-255
d256-262
d263-269
V251G
G
hGSDMD MGSAFERVVRRVVQELD-HGGEFIPVTSLQSSTGFQPYCLVVRKPSSSWFWKPRYKCVNL
mGSDMD MPSAFEKVVKNVIKEVSGSRGDLIPVDSLRNSTSFRPYCLLNRKFSSSRFWKPRYSCVNL
hGSDMD SIKDILEPDAAEPDVQRGRSFHFYDAMDGQIQGSVELAAPGQAKIAGGAAVSDSSSTSMN
mGSDMD SIKDILEPSAPEPEPECFGSFKVSDVVDGNIQGRVMLSGMGEGKISGGAAVSDSSSASMN
hGSDMD VYSLSVDPNTWQTLLHERHLRQPEHKVLQQLRSRGDNVYVVTEVLQTQKEVEVTRTHKRE
mGSDMD VCILRVTQKTWETMQHERHLQQPENKILQQLRSRGDDLFVVTEVLQTKEEVQITEVHSQE
hGSDMD GSGRFSLPGATCLQGEGQGHLSQKKTVTIPSGSTLAFRVAQLVIDSDLDVLLFPDKKQRT
mGSDMD GSGQFTLPGALCLKGEGKGHQSRKKMVTIPAGSILAFRVAQLLIGSKWDILLVSDEKQRT
hELANE
Caspase 1/11
hGSDMD FQPPATGHKRSTSEGAWPQLPSGLSMMRCLHNFLTDGVPAEG-AFTEDFQGLRAEVETIS
mGSDMD FEPSSGDRKAVGQRHHGLNVLAALCSIGKQLSLLSDGIDEEELIEAADFQGLYAEVKACS
mELANE
hGSDMD KELELLDRELCQLLLEGLEGVLRDQLALRALEEALEQGQS-LGPVEPLDGPAGAVLECLV
mGSDMD SELESLEMELRQQILVNIGKILQDQPSMEALEASLGQGLCSGGQVEPLDGPAGCILECLV
hGSDMD LSSGMLVPELAIPVVYLLGALTMLSETQHKLLAEALESQTLLGPLELVGSLLEQSAPWQE
mGSDMD LDSGELVPELAAPIFYLLGALAVLSETQQQLLAKALETTVLSKQLELVKHVLEQSTPWQE
hGSDMD RSTMSLPPGLLGNSWGEGAPAWVLLDECGLELGEDTPHVCWEPQAQGRMCALYASLALLS
mGSDMD QSSVSLPTVLLGDCWDEKNPTWVLLEECGLRLQVESPQVHWEPTSLIPTSALYASLFLLS
hGSDMD GLSQEPH
mGSDMD SLGQKPC

Figure S6. Related to Figure 6. Determination of ELANE cleavage site in mouse GSDMD. (A) Recombinant mouse His-SUMO-GSDMD was incubated with mELANE or mouse neutrophil lysates at 37°C for 30 min and subjected to SDS-PAGE followed by colloidal blue staining. The full length and ELANE-cleaved GSDMD N-terminal fragment were trypsin digested and analyzed by mass spectrometry (MS). **(B)** MS analysis of full length and ELANE-cleaved GSDMD. Trypsin digested peptides derived from the full length (blue lines) and ELANE-cleaved (red lines) mGSDMD are underlined. The putative ELANE cleavage sites are highlighted. **(C)** MS analysis of the ELANE cleavage site in mGSDMD was conducted using partially trypsin-digested samples. Top, mass spectrum of mGSDMD peptides generated through the cleavage. Bottom, MS/MS spectrum of the corresponding peptide showing the fragment ions detected/used for protein identification. MS analysis identifies V251 as the ELANE cleavage site in mGSDMD. **(D)** ELANE- and caspase-1-cleaved mGSDMD at different sites. The ELANE and caspase-1 cleavage sites as well as the peptide identified from the partially trypsin-digested sample are indicated. **(E-F**) Confirmation of ELANE cleavage site in mouse GSDMD. **(E)** The cleavage of mGSDMD deletion or point mutants by ELANE. The FLAG-tagged mGSDMD mutants were overexpressed in HEK293T cells. ELANE-mediated mGSDMD cleavage was carried out and analyzed as described in **Fig. S4J**. **(F)** Results of densitometry. Relative amounts of protein in **(E)** were quantified using NIH Image software as previously described. ELANE-elicited cleavage of mouse GSDMD was expressed as ratio of cleaved mGSDMD (mGSDMD-NT) and uncleaved full length mGSDMD (FL-mGSDMD). Results are the means (± SD) of three independent experiments. *, $P<0.01$ versus wild-type mGSDMD by Student's t test. **(G)** Comparison of the ELANE cleavage sites in human and mouse GSDMD. Human and mouse GSDMD amino acid sequences were aligned using Clustal Omega. Cleavage sites of Caspase 1 and ELANE are indicated with black arrow and red arrows, respectively.

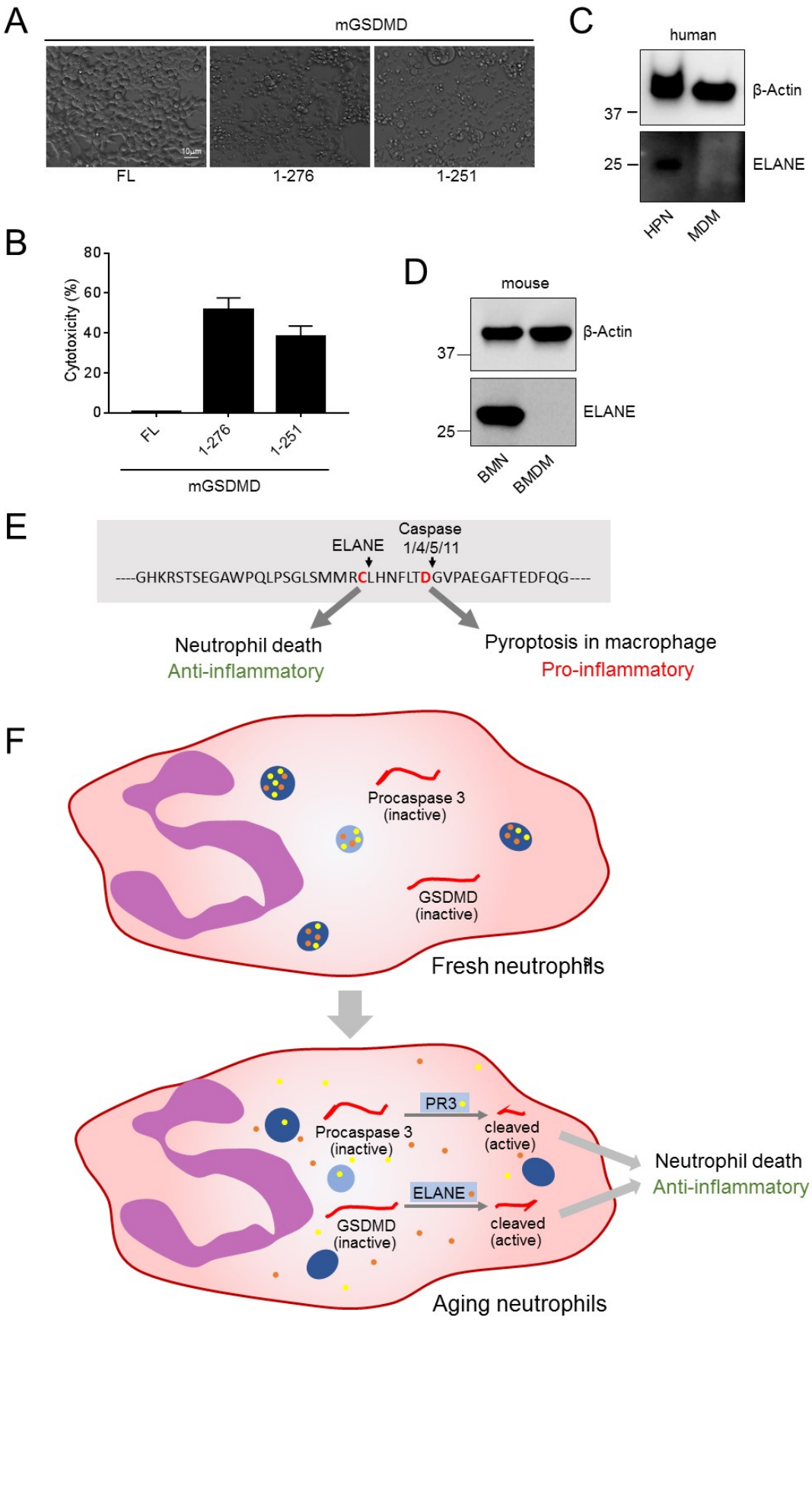
A
mGSDMD
FL
1-276
1-251
C
human
β-Actin
ELANE
37
25
HPN
MDM
B
Cytotoxicity (%)
80
60
40
20
0
FL
1-276
1-251
mGSDMD
D
mouse
β-Actin
ELANE
37
25
BMN
BMDM
E
ELANE
Caspase 1/4/5/11
----GHKRSTSEGAWPQLPSGLSMMRCLHNFLTDGVPAEGAFTEDFQG----
Neutrophil death
Anti-inflammatory
Pyroptosis in macrophage
Pro-inflammatory
F
Procaspase 3 (inactive)
GSDMD (inactive)
Fresh neutrophils
PR3
Procaspase 3 (inactive)
cleaved (active)
ELANE
GSDMD (inactive)
cleaved (active)
Neutrophil death
Anti-inflammatory
Aging neutrophils

Figure S7. Related to Figure 7. ELANE-induced cleavage of GSDMD is a key mechanism controlling neutrophil death. (A-B) ELANE-cleaved mouse GSDMD (mGSDMD-eNTs) are active and can lead to lytic cell death. HEK293T cells were transfected with the full-length mGSDMD or ELANE-cleaved N-terminal fragment (mGSDMD 1-251) expressing constructs. The analyses were conducted 24 h after transfection. **(A)** Cell morphology was assessed by brightfield microscopy. **(B)** Cytotoxicity was measured based on death-associated release of lactate dehydrogenase (LDH) according to the manufacturer's protocol. **(C-D)** Monocyte-derived macrophages do not express ELANE. **(C)** ELANE expression in human highly purified neutrophils (HPNs) and monocyte-derived macrophages (MDMs) was assessed by western blotting using an anti-ELANE antibody. **(D)** ELANE expression in mouse bone marrow neutrophils (BMNs) and bone marrow-derived macrophages (BMDMs) was assessed by western blotting. **(E)** GSDMD can exert context-dependent pro-inflammatory and anti-inflammatory effects. **(F)** Lysosomal membrane permeabilization (LMP) induced release of serine proteases from the granules to the cytosol mediates neutrophil death.

SUPPLEMTAL REFERENCES

Bajrami, B., Zhu, H., Kwak, H.J., Mondal, S., Hou, Q., Geng, G., Karatepe, K., Zhang, Y.C., Nombela-Arrieta, C., Park, S.Y*., et al.* (2016). G-CSF maintains controlled neutrophil mobilization during acute inflammation by negatively regulating CXCR2 signaling. J Exp Med *213*, 1999-2018.

Hattori, H., Subramanian, K.K., Sakai, J., and Luo, H.R. (2010). Reactive oxygen species as signaling molecules in neutrophil chemotaxis. Commun Integr Biol *3*, 278-281.

Jia, Y., Subramanian, K.K., Erneux, C., Pouillon, V., Hattori, H., Jo, H., You, J., Zhu, D., Schurmans, S., and Luo, H.R. (2007). Inositol 1,3,4,5-tetrakisphosphate negatively regulates phosphatidylinositol-3,4,5- trisphosphate signaling in neutrophils. Immunity *27*, 453-467.

Loison, F., Zhu, H., Karatepe, K., Kasorn, A., Liu, P., Ye, K., Zhou, J., Cao, S., Gong, H., Jenne, D.E*., et al.* (2014). Proteinase 3-dependent caspase-3 cleavage modulates neutrophil death and inflammation. J Clin Invest *124*, 4445-4458.

Luo, H.R., Saiardi, A., Yu, H., Nagata, E., Ye, K., and Snyder, S.H. (2002). Inositol pyrophosphates are required for DNA hyperrecombination in protein kinase c1 mutant yeast. Biochemistry *41*, 2509-2515.

Mondal, S., Ghosh-Roy, S., Loison, F., Li, Y., Jia, Y., Harris, C., Williams, D.A., and Luo, H.R. (2011). PTEN negatively regulates engulfment of apoptotic cells by modulating activation of Rac GTPase. J Immunol *187*, 5783-5794.

Sakai, J., Li, J., Subramanian, K.K., Mondal, S., Bajrami, B., Hattori, H., Jia, Y., Dickinson, B.C., Zhong, J., Ye, K*., et al.* (2012). Reactive oxygen species-induced actin glutathionylation controls actin dynamics in neutrophils. Immunity *37*, 1037-1049.

Subramanian, K.K., Jia, Y., Zhu, D., Simms, B.T., Jo, H., Hattori, H., You, J., Mizgerd, J.P., and Luo, H.R. (2007). Tumor suppressor PTEN is a physiologic suppressor of chemoattractant-mediated neutrophil functions. Blood *109*, 4028-4037.